Spring 1-1-2020

Noncovalent Complexation of Single-wall Carbon Nanotubes With Biopolymers: Dispersion, Purification, And Protein Interactions

Ana Dilillo
Cleveland State University

NONCOVALENT COMPLEXATION OF SINGLE-WALL CARBON NANOTUBES WITH BIOPOLYMERS: DISPERSION, PURIFICATION, AND PROTEIN INTERACTIONS

ANA DILILLO

Bachelor of Chemical Engineering

Cleveland State University

May 2020

Submitted in partial fulfillment of requirements for the degree

MASTER OF SCIENCE IN CHEMICAL ENGINEERING

at the

CLEVELAND STATE UNIVERSITY

MAY 2021

We hereby approve the thesis for

ANA DILILLO

Candidate for the Master of Science in Chemical Engineering degree for the

Department of Chemical and Biomedical Engineering

And CLEVELAND STATE UNIVERSITY'S

College of Graduate studies by

Thesis Chairperson, Dr. Geyou Ao

Department of Chemical and Biomedical Engineering

4/30/2021

Thesis Committee Member, Dr. Xue-Long Sun

Department of Chemistry

4/30/2021

Thesis Committee Member, Dr. Moo-Yeal Lee

Department of Chemical and Biomedical Engineering

4/30/2021

Date of Defense: April 27, 2020

ACKNOWLEDGMENTS

First and foremost, I want to express my gratitude to Dr. Geyou Ao for giving me the opportunity to join her BioNano Materials Lab. You have not only guided my development in research but also acted as my mentor and I am extremely grateful. Over these years, you have constantly pushed me to strive for excellence, and I have found myself constantly surpassing what I believed my capabilities to be under your tutelage. Thank you for guiding me on my academic and professional path.

I would like to thank Dr. Xue-Long Sun and Dr. Moo-Yeal Lee for offering their constructive feedback on my thesis and guiding me to excel in my academic achievements. I would like to express my appreciation to the facility and research associates in both the Chemical and Biomedical Engineering Department and Chemistry Department for all of your guidance along the way.

Thank you to my lab mates for making every day enjoyable and fun. You have all been there to support me during my research and celebrated my achievements with me. I look forward to seeing all of us grow as professionals and remain connected through the future.

Thank you, Katherine, you have been a constant support in my life, and I could never ask for a more thoughtful, and caring friend.

Most importantly, thank you to my family, for your unconditional love and support. You have continued to support me through my extensive academic career and have helped me to grow as a person. Thank you for teaching me to never give up on my dreams and the importance of hard work.

NONCOVALENT COMPLEXATION OF SINGLE-WALL CARBON NANOTUBES WITH BIOPOLYMERS: DISPERSION, PURIFICATION, AND PROTEIN INTERACTIONS

ANA DILILLO

ABSTRACT

This thesis is a comprehensive study on the noncovalent complexation of single-wall carbon nanotubes (SWCNTs) using biopolymers, including single-stranded DNA and synthetic glycopolymers to explore their potential applications as optical sensors. SWCNTs are cylindrical structures of carbon lattice with diameters of ≈ 1 nanometer. They have unique electronic, chemical, and optical properties, which make them ideal candidates for bioimaging, biosensing, and drug delivery applications. The resulting biopolymer-SWCNT complexes maintain the intrinsic properties of nanotubes and possess specific biological functionalities as well.

Here, we have extensively studied the structure-property relationship of two types of biopolymer-complexed SWCNT systems, namely DNA- and glycopolymer-wrapped SWCNTs (i.e., DNA-SWCNTs and Glyco-SWCNTs). First, we investigated the optical properties of DNA-SWCNTs utilizing $(GT)_n$ sequences, where n = 6, 10, 15, 20, at controlled pH to examine the effect of DNA nucleobase deprotonation on the near-infrared (NIR) fluorescence of SWCNTs and the subsequent SWCNT separation. When increasing the pH of aqueous dispersions of DNA-SWCNTs to a basic region (i.e., pH ≈ 12) the NIR emission intensity of nanotubes increased indicating the conformational change of DNA on the surface of nanotubes. The resulting DNA-SWCNT complexes distributed unevenly in a polymer aqueous two-phase system, allowing SWCNT separation at controlled pH.

Next, we studied Glyco-SWCNT complexes and their ability to interact with carbohydrate-binding proteins (i.e., lectins). We utilized a disaccharide lactose-containing homopolymer with a polymer chain length of n = 400 (i.e., Lact-AM 400) to investigate the dispersion quality and carbohydrate-protein binding interactions of Glyco-SWCNTs. Various lectins were utilized including glucose and mannose-binding *Concanavalin A* (ConA) and galactose-binding *Arachis hypogaea* (PNA) to determine carbohydrate-protein interactions which were compared to mannose-binding *Galanthus nivalis* (GNA) and Bovine serum albumin (BSA) that does not bind specifically to carbohydrates. ConA showed a greater ability to cause the cross linking and aggregations of Glyco-SWCNTs while PNA reacted faster with Glyco-SWCNTs based on the kinetics of protein interactions.

Taken together, our findings provide insights for creating biopolymer-SWCNT complexes with controlled optical properties and biological functionalities. This opens new possibilities for designing novel nanosystems for many applications, from nanotube purification to biological sensing and imaging to nanomedicine.

TABLE OF CONTENTS

Page

LIST OF TABLES

Table Page

LIST OF FIGURES

Figure Page

CHAPTER I

INTRODUCTION

Single-wall carbon nanotubes (SWCNTs) have been the topic of extensive study for the past thirty years due to their unique electronic, chemical, and optical properties making them excellent candidates for bioimaging, bioelectronics, and drug delivery.[1–10] SWCNTs are cylindrical nanostructures comprised of a single atomic layer of sp^2 hybridized carbon lattices with diameters of approximately 1 nm.[1–3] They are being widely researched as fluorescent probes for bioimaging and biosensing due to their intrinsic photoluminescence in the near-infrared (NIR) region.[7,8,11–14] Additionally, due to their single atom thickness, they have maximum surface contact with their surrounding environment making them ideal for surface functionalization and drug delivery systems.[8,13,14]

SWCNTs are characterized based on the chiral angle and chiral vector giving them unique chiral integers of (n, m) that directly correlate to tube diameter and electronic structures.[2,15,16] Each semiconducting SWCNT species has its unique band gaps between the valence and conductive bands that are designated by E_{ii} (i=1,2,3,…).[15–17] These band gaps render different SWCNT species distinct optical transition peaks in absorption and

NIR fluorescence measurements. Therefore, utilizing SWCNTs of well-defined structure and property is required for many applications, particularly in biological sensing and imaging. Extensive research has been conducted to separate single-chirality SWCNTs from a synthetic SWCNT mixture. Techniques such as aqueous two-phase (ATP) separation, gel chromatography, and ion exchange chromatography are among the most popular separation methods.[18–23]

In this thesis, we have demonstrated the noncovalent complexation of SWCNTs using biopolymers, including single-stranded DNA and glycopolymers, to study the effects of pH-controlled environments on the optical property and purification of DNA-SWCNTs and the interactions between carbohydrate-binding proteins and Glyco-SWCNT complexes. First, we examined the optical properties of DNA-wrapped SWCNTs at controlled-pH, particularly the NIR fluorescence of nanotubes, to determine the effect of nucleobase deprotonation in a basic region on the changes in the DNA wrapping structure around the surface of nanotubes. Specifically, we utilized $(GT)_n$ DNA sequences, where n=6, 10, 15, 20, to disperse SWCNTs in water and characterized the optical properties of nanotubes in a wide range of solvent pH = 1-13. Guanine nucleobase has unique first and second deprotonation pKa of 9.19-10.03 and >11.94 pH respectively, potentially promoting the hydrogen bonding between DNA bases in the basic region.[24,25] At pH 12, the deprotonation of guanine led to up to 7-fold increase in the NIR fluorescence of SWCNTs at a wavelength of 1140nm, corresponding to that of the large diameter species (8,4) in the starting materials. The DNA conformational changed based on the solvent pH further enabled the partition of specific DNA-SWCNTs in a polymer aqueous two-phase (ATP) system for nanotube separation. This provides insights for utilizing the protonation

or deprotonation of DNA bases by pH to modulate the DNA wrapping structure around the nanotube to further tune nanotube properties.

Second, we explored the complexation of SWCNTs with a disaccharide lactose-containing homopolymer to form water-soluble Glyco-SWCNT complexes, that can interact specifically with carbohydrate-binding proteins (i.e., lectins). Carbohydrate-protein interactions are extensively seen in plant, animal, bacterial, and viral cells. They are responsible for numerous cellular events, such as cancer metastasis, cell-cell adhesion, and cell differentiation.[14,26–28] Lectins display both mono- and multivalent interactions depending on the number of binding sites present; however, monovalent carbohydrate ligands have relatively weak binding due to primary forces being a combination of hydrophobic and electrostatic interactions and hydrogen bonding.[26] By increasing multivalent interactions through multiple carbohydrates in a close proximity, we are able to accumulate these weak forces into a strong binding force. This has made synthetic glycopolymers a novel approach to study carbohydrate-lectin interactions due to their tunable sugar densities and multivalency.[14] Nanomaterials further accommodate the high-density ligands due to their nanoscale sizes and high specific surface areas, thereby promoting multivalent interactions of glyconanomaterials with proteins. In addition, carbohydrate-lectin interactions on cell surfaces form cross-linking lattices that have made precipitation and agglomeration techniques suitable for researching the specific binding affinity.[27,29–31] We have explored the kinetics of Glyco-SWCNT interactions with various lectins of variable carbohydrate binding affinity and the resulting nanotube aggregation behavior to gain a deeper understanding of the targeted interactions of carbohydrate-protein pairs.

This thesis summarizes research on the noncovalent complexation of SWCNTs with biopolymers (i.e., DNA and glycopolymer), optical properties of nanotubes, and applications in carbon nanotube sorting at controlled pH and optical sensing of carbohydrate-protein interactions. Chapter II provides background information on materials used, including SWCNTs, DNA, glycopolymers, and fluorescence. Chapter III details research performed on the optical characterization of DNA-wrapped SWCNTs at controlled pH including methods, results, and discussion. Chapter IV details research conducted for the carbohydrate-protein binding interactions on noncovalent Glyco-SWCNT complexes including methods, results, and discussion. Chapter V is a summary conclusion of the thesis in its entirety, and Chapter VI and VII are references and appendix, respectively.

CHAPTER II

BACKGROUND

1 History

Carbon nanotubes (CNTs) have quickly become a leading research material in biotechnology due to their unique physical, chemical, and optical properties. However, the discovery of CNTs occurred accidentally as a byproduct of fullerene synthesis. In 1990 Yoshinori Ando was mass producing fullerenes and decided to attempt switching the process from using AC arc discharge to DC arc discharge. This experimental change resulted in fullerenes accompanied by what looked like a mass of "carbon soot".[32] Ando supplied this soot covered cathode to his friend Sumio Iijima who discovered they were CNTs in 1991 and started nanocarbon research from there.[3,32] Ando may be responsible for producing the first CNTs; however, Iijima cultivated the knowledge by determining nanometer-order diameter and cylindrical graphite helical arrangement through extensive observation and research.[32] The initial CNTs studied by Iijima were multi-wall carbon nanotubes (MWCNTs); however, Iijima and his group at NEC Laboratory were able to synthesize single-wall carbon nanotubes (SWCNTs) within two year.[3]

2 Single-wall Carbon Nanotubes

2.1 Synthesis of SWCNTs

In the beginning, there were three main methods for synthesizing CNTs: arc discharge, laser ablation, and chemical vapor deposition (CVD). Today, CVD is widely used for synthesizing SWCNTs because it offers the best production control of chirality and diameter.[33] CVD refers to a method were CNTs are grown when hydrocarbon gases are dissociated on catalysts at high temperatures (600-1200 °C).[34] Two of the most popular methods of CVD synthesis are: high-pressure carbon monoxide (HiPco) gas-phase synthesis and CoMoCAT, which uses methane to grow SWCNTs on alumina supported Co-Mo catalysts. Both methods produce CNTs with a high selectivity towards SWCNTs, but results in a mixture of metallic, quasi-metallic, and semiconducting SWCNTs along with metal catalyst impurities. The impurities can be removed during the dispersion process and separation techniques are utilized to isolate semiconducting SWCNTs to ensure fluorescent properties in samples.[33] CVD refers to a method were CNTs are grown when hydrocarbon gases are dissociated on catalysts at high temperatures (600-1200 °C).[34] Two of the most popular methods of CVD synthesis are: high-pressure carbon monoxide (HiPco) gas-phase synthesis and CoMoCAT, which uses methane to grow SWCNTs on alumina supported Co-Mo catalysts. Both of these methods produce CNTs with a high selectivity towards SWCNTs, but results in a mixture of metallic, quasi-metallic, and semiconducting SWCNTs along with metal catalyst impurities. The impurities can be removed during the dispersion process and separation techniques are utilized to isolate semiconducting SWCNTs to ensure fluorescent properties in samples.

2.2 Fundamental Properties of SWCNTs

In order to understand SWCNTs, an in depth look at the structure and properties of the CNT must be discussed. It is the easiest to imagine a flat sheet of graphene comprised of sp^2 bonded carbon atoms rolled up to form a cylinder. Now keep in mind, when rolling a sheet, you can change the angle of rolling, chiral angle, and the diameter of the final cylinder. These properties have an immense impact on the final properties (physical, electronic, optical, etc.) of the SWCNT. The final nanotube is comprised of a cylinder of one atom thick bound carbon atoms with fullerene caps at the end.[1] The carbon atoms are covalently bound to three neighboring carbons via σ-bonds, while the remaining p-electron forms a π-electron system responsible for the SWCNT electronic and optical properties.[15] The chiral angle and the tubule diameter is dependent on the chiral vector, which is defined as the integers (n,m), and the vector length, L.[1,3] The chiral angle results in three distinct nanotube structures: zigzag, armchair, and chiral. The zigzag, armchair, and chiral nanotube conformations correspond to the chiral angles of 0°, 30°, and $0^\circ < \theta < 30^\circ$, respectively (Figure 2.1).[3]

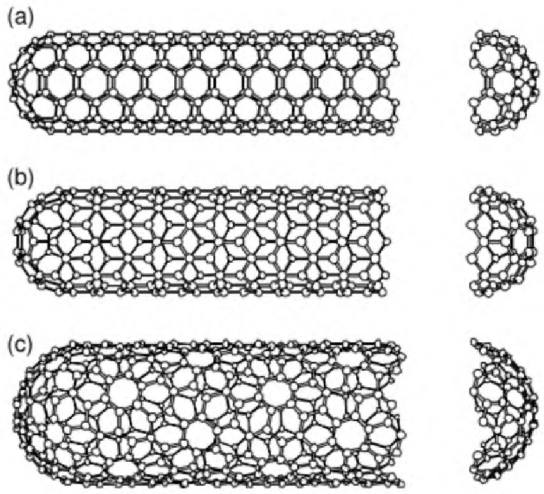

Figure 2.1: Schematic models of single-wall carbon nanotubes with the chiral angles corresponding to (a) armchair (b) zigzag and (c) chiral structures. Reproduced from Ref (1,3).

In addition to the chiral angle, the vector integers, (n,m) play a vital role in determining the electronic properties of the SWCNT. These vector angles signify the "species" of the carbon nanotube and can confirm the chiral angle and electronic properties. Zigzag configured nanotubes will have integers valued at (n, 0) or (0, m), while armchair configurations will have a vector of (n, n).[3] Both zigzag and armchair configurations result in achiral nanotubes (Figure 2.2).[15]

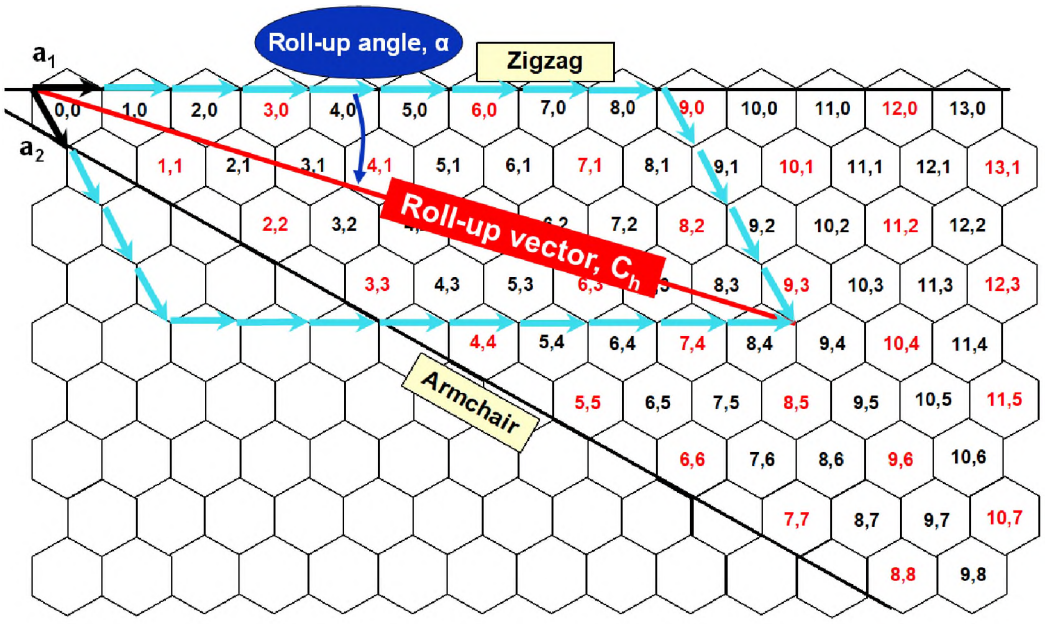

Figure 2.2: Schematic depicting the dependence on chiral angle and vector integers on SWCNT species. Reproduced from Ref (15).

The vector integers (n,m) can also be used to determine if a SWCNT species is metallic, quasi-metallic, or semiconducting. This plays a vital role in the optical characteristics of the nanotube, which will be discussed later. Armchair configurations where n = m display Fermi energy states and therefore a metallic electronic behavior.[15] When n-m is divisible by 3, the nanotubes display quasi-metallic properties due to band gaps being present by very small (i.e., 0.03 - 0.08 eV). All of the remaining species are semiconducting SWCNTs which possess unique band gaps in the range of roughly 0.8 – 1.9 eV that vary with the diameter of the nanotube.[15] The semiconducting SWCNTs are the main focus of the research conducted within this thesis due to the unique electronic signatures created by the present band gaps. The unique electronic signatures allow the characterization of SWCNT species, concentration, and interactions through the study of absorbance and fluorescence profiles.

The species determination of a SWCNT not only effects the optical properties but also the physical properties displayed. SWCNT length can vary from 100 nm to 100,000 nm. Theoretically, SWCNTs should possess intrinsic tensile strengths in the range of 100-200 GPa; however, experimental data displays lower results due to defects and shows a strong dependence on chiral structure and diameter.[35] Small-diameter, armchair structured nanotubes exhibit the highest tensile strength experimentally, but it is difficult to test the extent of species correlation due to the hardship of performing tests on an isolated single species of SWCNT. Takakura et al proceeded to test the tensile strength of 16 unique species and summarize chirality dependence.[35] His work determined the tensile strength ranging from 25-66 GPa, which is a fraction of the theoretical value due to structural defects such as: atomic vacancies, topological defects, or helical structural defects.[5,35,36] This is approximately 50x greater than the tensile strength of steel. SWCNTs also display impressive electrical and thermal conductivity up to 10,000 S/cm and 6,000 W/m· K respectively.[4,6,37] To put this in perspective, diamond has a thermal conductivity of 1,000 W/m· K and copper has an electrical conductivity of 596,000 S/cm.

3 Single-Wall Carbon Nanotube Dispersion

SWCNT raw material powder is comprised of bundles of SWCNTs of various species and metallic impurities that are insoluble in aqueous environments. The raw powder is unfit for application and biological environments which is why SWCNTs undergo dispersion techniques to facilitate: separation of SWCNT species, preparation for devices, preparation for SWCNT composites, environmental and toxicology studies, and preparation for functionalization.[10,38–41] The separation of unique species allows for the specific NIR fluorescence to be utilized in biosensors and bioimaging, while the suspension

in aqueous environments prepares the SWCNTs for biological environments. In addition, dispersion techniques allow us not only to break up the SWCNT bundles but also to remove any impurities present in the raw powder.

The solubilization of SWCNTs can be conducted via covalent or noncovalent functionalization. Noncovalent surface complexation of SWCNTs can be carried out using biopolymers (glycopolymers, oligomers, etc.), surfactants, and small molecule complexing agents, while covalent functionalization methods include: diazonium reactions, reductive alkylation's, nitrene additions, and halogenations.[38,42] Covalent and noncovalent functionalization have immense effects on the properties of the SWCNT. Noncovalent functionalization retains the π-electron system of the carbon latticework, but it proves difficult to maintain stability over long periods of time; however, covalent functionalization has high stability through strong bonds but eliminates the π-electron system in favor of sp^3 sites leading to diminished properties.[43] The research provided here will focus on the noncovalent functionalization of SWCNTs through deoxyribonucleic acid (DNA) and glycopolymer wrapping.

The most common method for nanotube dispersion is sonication in an aqueous environment. The sonication allows for the nanotube bundles to break apart so that maximum surface interactions are available. There are two major drawbacks to the sonication method for dispersion. First, the length of the SWCNTs is shortened due to damage of the carbon lattice structure. Second, sonication results can be difficult to reproduce and even more difficult to scale-up for industrialization. Additional methods for dispersion exist such as ball mill and shear force mixer showing varied efficiency but greater retention of SWCNT length.[39]

3.1 DNA-Wrapped SWCNTs

Noncovalent complexation of SWCNTs using biomolecules (e.g., proteins/enzymes, antibodies/antigens, and oligomers) to form hybrid complexes is a favorable method because it combines the fluorescent and physical properties of the semiconductive SWCNT with the biorecognition of the biomolecule.[10,41] Biomolecule-SWCNT hybrids allow for the application in biosensors, bioimaging, and nanobioelectronic systems.[10] The method used in our research utilizes DNA-wrapped SWCNTs to explore the effects of controlled pH on the optical properties of the SWCNT.

Single-stranded DNA (ssDNA) has proven to be an efficient dispersant for SWCNTs because the ssDNA can adsorb onto the nanotube surface to form a stable aqueous dispersion due to van der Waals and hydrophobic forces. The ssDNA wraps around the SWCNT due to the hydrophobic nucleic bases adsorbing to the surface causing π-π stacking. While the hydrophobic nucleobases are adsorbing to the surface, the hydrophilic sugar phosphate backbone is free to interact with the aqueous environment.[10,38,41,44] The hydrophilic sugar phosphate backbone allows for the DNA-SWCNT hybrid to become soluble in an aqueous environment and shows high stability through electrostatic interactions. Empirical studies, molecular dynamic simulations, and transmission electron microscopy (TEM) images have proven that DNA wraps helically around the SWCNT and this helical wrapping structure is retained even during the drying process (Figure 2.3).[8,20,44,45]

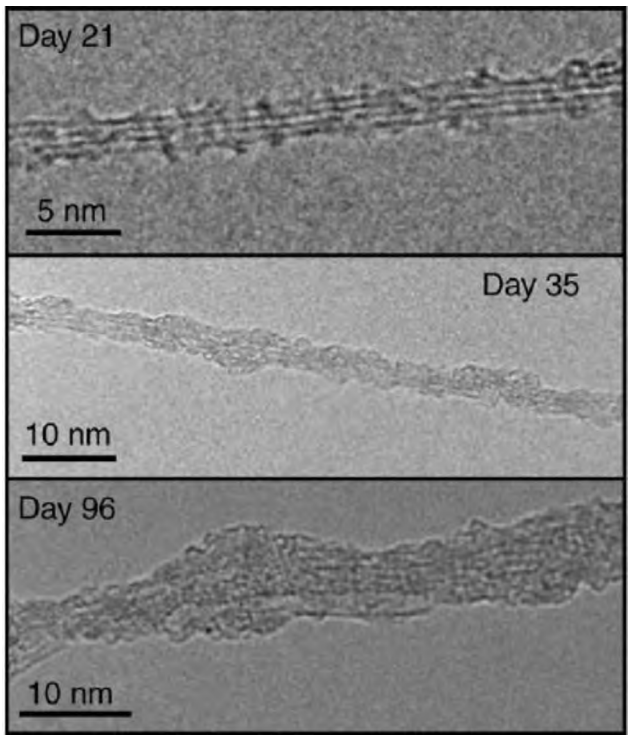

Figure 2.3: Various HRTEM images depicting the helical structure of DNA-wrapped SWCNTs with increased adsorption over time. Reproduced from Ref (8).

Furthermore, DNA has shown the ability to separate out distinct nanotube chiralities due to the unique recognition between specific ssDNA oligomers with specific (n, m) nanotube species. The recognition DNA sequences exhibit a distinct hydrophobicity/charge density linked to a specific nanotube species. It is hypothesized that the DNA wrapping structure around the nanotube surface is stabilized by hydrogen-bonding networks occurring between the adsorbed nucleobases.[22,46] The differences in hydrophobicity for recognition DNA-SWCNT pairs aid separation of single species through techniques such as gel chromatography and aqueous two-phase polymer separation which rely on hydrophilic/hydrophobic split environments.

3.2 Glycopolymer-Wrapped SWCNTs

Polymers can also be used for the noncovalent complexation with SWCNTs. Polymer-wrapped nanotubes occur due to a variety of concurrent interactions including van der Waals attractions, multivalent π-π stacking, and hydrophobic interactions.[13,26,47,48] Additionally, polymers can be used for covalent functionalization of nanotubes via the "grafting from" and "grafting to" techniques.[13] The focus of this thesis relies on the noncovalent functionalization of polymers to SWCNTs. The resulting polymer-wrapped SWCNT hybrids are water soluble and allow for additional functional groups attached via the polymers. The functional attachment explored here will be pendant carbohydrates attached to a polymer backbone forming glycopolymers.

3.2.1 What are Glycopolymers?

Glycopolymers are synthetic polymeric structures with pendant sugar groups, which mimic the role of glycoproteins, glycolipids, and glycans in cell membranes. Glycopolymers are capable of mimicking natural glycoconjugates due to their capability for multivalent interactions with carbohydrate-binding proteins, lectins.[14,26,47,49] Glycopolymer can be synthesized through direct polymerization of vinyl glycomonomers or post-modification of polymers with carbohydrate-containing compounds.[49–52] Both methods for glycopolymer synthesis are extensive and time-consuming due to the elaborate chemical requirements of carbohydrate preparation requiring multistep reactions to protect and deprotect the hydroxyl groups on the carbohydrate.[49,51] A key goal in glycopolymer synthesis is to maximize pendant carbohydrate ligands so that multivalent interactions with proteins form strong bonds. Additionally, variant polymers have been researched to explore the binding capabilities of glycopolymers utilizing linear and hyperbranched

polymer backbones in an effort to increase multivalent interactions.[48] Glycopolymers have shown promise in functionalizing nanotubes and nanoparticles via covalent and noncovalent functionalization. These water-soluble glycopolymer-wrapped nanomaterials have immense potential in tissue engineering, bionanotechnology, and pathogenic bioimaging. In order to understand the role of glycopolymers in nanotechnology, one must first explore the importance of glycan-protein interactions.

3.2.2 Glycan-protein interactions

Cell surfaces are covered with a variety of receptors that are responsible for numerous cellular events, such as cell-cell adhesion, cell recognitions, cancer metastasis, and intercellular communication.[14,26,49] Cellular events occur via glycan (carbohydrate)-protein, protein-protein, and antigen-antibody interactions. Proteins capable of recognizing specific glycans are referred to as lectins, which can be found in plants, animals, bacteria, and viruses.[27] Lectins contain two or more carbohydrate-binding sites and are responsible for agglutination of cells and precipitation of glycoconjugates.[49] Due to the carbohydrate-binding sites, lectins are capable of binding to glyconanostructures, glycopolymers, and glycopeptids. Glycan-protein binding occurs via a combination of hydrogen bonding and hydrophobic interactions and can occur both monovalent and multivalent depending on the protein recognitions sites and the structure of carbohydrate ligands, such as the glycan density and spatial conformation; however, monovalent binding is much weaker than its multivalent counterpart (Figure 2.4).[31,49] Monovalent carbohydrate-protein interactions have a dissociation constant (K_d) in the order of millimolar compared to the strong multivalent interactions with a value in the order of micromolar.[26] Due to this,

glycopolymers are synthesized to maximize the multivalent effect via multiple binding ligands, or "glycoclusters".[26]

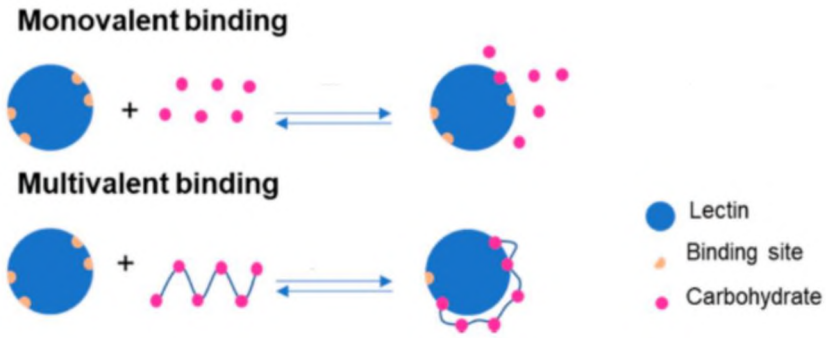

Figure 2.4: Schematic of monovalent and multivalent carbohydrate-lectin binding. Reproduced by Ref (48).

4 Fluorescence Characterization

4.1 NIR Fluorescence of SWCNTs

Semiconducting SWCNTs have unique electron band gaps that vary inversely with nanotube diameter giving each species a unique fluorescent signature. The optical and electronic structure of SWCNT is dependent on the traverse structure therefore the absorbance and fluorescent signature for each species is independent of length variation.[2,15] The band gap is a result of dipole-allowed transitions of polarized light from a valence sub-band to a corresponding conduction sub-band resulting in van Hove singularities.[15,17] The van Hove singularities result in a series of unique sharp peaks indicative of specific energies, E_{ii}, where i is given value 1, 2, 3, … to represent the sub-bands (Figure 2.5).[15,17] Semiconducting SWCNTs are unique because the three optical transition peaks occur in the near-infrared, visible, and near-ultraviolet region, while metallic and quasi-metallic SWCNTs begin their transitions in the visible region. Additionally, metallics display

overlapping of the valence and conducting sub-bands eliminating a fluorescent signature. Although the van Hove singularities are present at unique wavelengths for each SWCNT species, they do fall near each other. This results in samples with multiple species displaying overlapping and broadened peaks. Through the separation of semiconducting (n, m) species, we can isolate distinct peaks and as a result specific correlating fluorescent colors. The SWCNT photoluminescence is extremely sensitive to local environments with parameters, such as pH and functionalization compound, resulting in peak intensity variation and wavelength shifts. The NIR photoluminescence of SWCNTs is unique due to its stability, tunability, and sensitivity giving them promising potential for biosensors and optical probes.

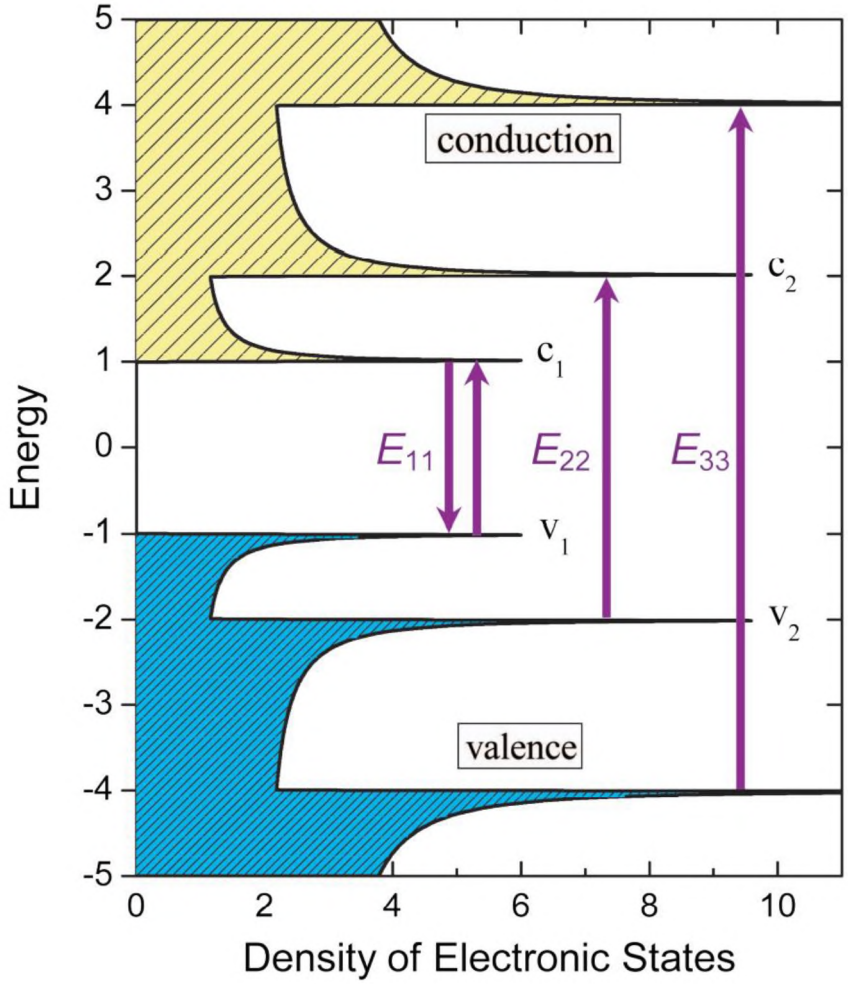

Figure 2.5: Schematic of semiconducting SWCNT band gap theory depicting the transition states responsible for van Hove singularities. Reproduced from Ref (52).

4.2 Visible Fluorescence of FITC Marker

Fluorescein isothiocyanate (FITC) is the most widely used fluorescence labelling reagent for experimentation and is often conjugated to proteins due to its unique absorption/emission properties and high conjugate stability.[53,54] FITC labelling occurs due to the fluorophore absorbing light resulting in excitation of electrons. The electrons are excited from their resting state (S_0) to an energy level called the excited electronic singlet state (S_2). [55] As the fluorophore exhibits conformational changes, the electrons drop to the

electronic single state (S_1) referred to as the Stokes shift. Finally, electrons drop back to their resting state resulting in a release of energy as fluorescence ($E_{Emission}$) (Figure 2.6).[55] For FITC, the emission wavelength is in the visible region with a maximum at 525 nm.

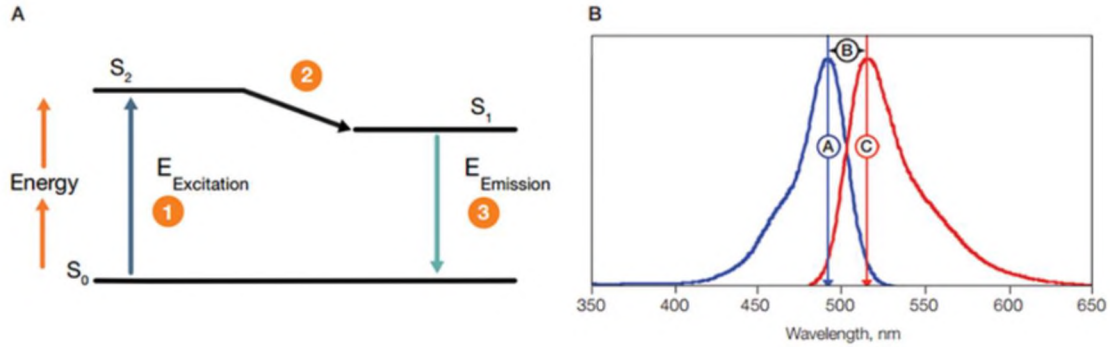

Figure 2.6: (A) depicts the electron excitation of a fluorophore and the Stokes shift that occurs before emission. (B) shows the effect of Stokes shift on fluorescence spectra with peak C corresponding to FITC maximum emission peak. Reproduced from Ref (55).

FITC is widely used for protein labeling due to its ability to react with a protein's primary amine via a covalent amide bond resulting in a FITC-protein conjugate.[53] In order to efficiently utilize FITC for protein marking, samples require a highly pure, highly concentrated protein. It is important to note the use of FITC marked proteins for carbohydrate-protein reactions is not a "turning on" of the fluorescent marker but rather a quenching effect. As the fluorophore-conjugated protein undergoes conformational changes the fluorophore undergoes quenching which diminishes the emission strength.[54] Analysis of the diminishing fluorescence marker over time directly corresponds to the binding interactions occurring between carbohydrates and proteins. The quenching phenomena allows us to determine glycan-protein binding kinetics for different proteins.

CHAPTER III

OPTICAL CHARACTERIZATION AND PURIFICATION OF DNA-WRAPPED SINGLE-WALL CARBON NANOTUBES AT CONTROLLED PH

1 Introduction

Single-wall carbon nanotubes (SWCNTs) are cylindrical structures of carbon atoms displaying unique mechanical, electronic, chemical, and optical properties.[2,4–6,35,37] These extraordinary properties allow for a wide range of application, such as bioimaging, biosensing, and electronics.[7,12,28,56] They are the subject of extensive studies involving both *in vitro* and *in vivo* interactions with chemicals and biomolecules. SWCNTs are characterized as species (*n*,*m*) defined by their diameter and chiral angle. In order to be used efficiently in future applications, SWCNTs require purification into single chirality-based species with unique optical and electronic properties, particularly their intrinsic photoluminescence in the near-infrared (NIR).[1–3] The unique electronic signature is the result of electron transitions from valence band to conduction band.[15,16] These band gaps are referred to as the van Hove singularities, identified as E_{ii} (i=1,2,3,…). These band gaps are unique to semiconducting nanotubes and all fluorescence properties are dictated by the

E_{11} singularity.[15,16] Semiconducting SWCNTs fluoresce in the NIR between approximately 900 to 1600 nm allowing for deep tissue penetration, which is ideal for biological samples.[7] Purification is crucial due to non-specific synthesis and dispersion methods. Numerous methods of purification have been studied including DNA-based separation, aqueous two-phase extraction (ATP), and gel chromatography.[18–21,23,45]

Prior to purification, SWCNTs require dispersion in a solvent to remove carbonaceous impurities, metal catalyst particles, and disperse aggregated bundles bound by van der Waals forces.[38,40,41,45] Our approach utilizes single-stranded DNA (ssDNA) sequences folded on the surface of the SWCNT resulting in DNA-wrapped SWCNT hybrids. The complex nature of ssDNA allows for noncovalent functionalization of SWCNTs due to the π-π stacking of the hydrophobic nucleobases. Additionally, the hydrophilic and negatively charged phosphate backbone allows the SWCNTs to be stably dispersed in an aqueous environment.[57] Target DNA sequences are utilized to recognize specific (*n*, *m*) species with unique NIR signals. Additionally, DNA nucleobases are pH sensitive and display site-specific deprotonation, unique to each nucleobase, which potentially promotes hydrogen bonding between the DNA nucleobases and SWCNT surface; therefore, causing conformational changes.[24,25] These conformational changes may increase the shielding of quenching species in solvent from the surface of the SWCNT allowing for increased fluorescence emission. Subsequently, the conformational changes alter the hydrophobicity of DNA-wrapped SWCNT hybrids allowing for varied ATP separation at precise pH levels. Additionally, the alkalinity of solvent correlates with the redox chemistry of SWCNTs.[58] Acidic conditions readily oxidize large diameter

SWCNTs, while alkaline conditions reduce oxidation potential.[58] The reduction potential directly effects the NIR fluorescence potential of large diameter SWCNTs.

The premise of this research is to determine the effects of controlled pH on the dispersion and separation process of DNA-wrapped SWCNTs. Sequence-controlled $(GT)_n$ (n = 6, 10, 15, 20) DNA are used to determine the effects of controlled pH (1-13) on the optical properties and separation outcome of SWCNTs that are wrapped by ssDNA with varying lengths. The site-specific second deprotonation of guanine (G) occurs at pH ≈ 12, which promotes hydrogen bonding to stabilize the wrapping structure of DNA and increases shielding of nanotubes from the solvent environment resulting in increased fluorescence emission of the SWCNT.[24,59] The optimal pH, 12, was used to study the effects of SWCNT and free DNA concentration to determine the saturation level of increased interactions. Additionally, further experiments were conducted altering the pH prior to dispersion resulting in similar yield while increasing dispersion quality. Lastly, ATP separation was conducted using polyethylene glycol and dextran at a broad range of pH (1-13) with the addition of polyvinylpyrrolidone. Unique species separation from a supernatant dispersion of SWCNTs was observed at different pH levels, demonstrating that controlled pH can further allow the purification of high-purity single-chirality SWCNTs with unique optical properties.

2 Materials and Methods

SWCNTs (CG100, CoMoCAT) were purchased from CHASM Advanced Materials. Custom DNA oligos (GT)n (n=6,10,15,20) were purchased from Integrated DNA Technologies, Inc. (Coralville, Iowa). Dextran 70 (DX) (MW = 70,000, Tokyo Chemical Industry Co.), polyvinylpyrrolidone (PVP) (MW = 10,000 Sigma Aldrich),

polyethylene glycol (PEG) (MW = 6,000, Alfa Aesar), sodium hydroxide (NaOH) (MW = 40,000, Sigma Aldrich), hydrogen chloride (HCl) (SG 1.19, normality 12.1, Fisher Chemical), sodium chloride (NaCl) (Sigma Aldrich) were utilized.

For dispersion of SWCNTs with DNA sequence, 1 mL of SWCNT and DNA mixture (2 mg DNA, 1 mg SWCNT) in deionized (DI) water with 0.1 M NaCl was tip sonicated in an ice bath (model VCX 130, Sonics and Materials, Inc.) for 2 hours at 8 W power level. After centrifugation at 17000g for 90 min at 20 ± 2 °C, the supernatant of DNA-wrapped SWCNT dispersion is collected. All $(GT)_n$ supernatants were tested at 20x dilution and fluorescence was tested using NS3 NanoSpectralyzer (Applied NanoFluorescence). The supernatant was diluted to 20.0 ± 5.0 μg/mL using the extinction coefficient 0.04163 L/mg·cm at 780 nm.[60] The diluted samples are tested at wide range pH (1-13) through the addition of small aliquots of NaOH and HCl (~3.0 μL) per 150 μL sample using Mettler Toledo table-top pH meter. UV-vis-NIR absorbance and fluorescence measurements were performed using NS3 NanoSpectralyzer over the wavelength range of 400-1600 nm using a 1 cm path length quartz cuvette.

SWCNT to DNA mass ratio was tested for $(GT)_6$ using a ratio 1:n (n = 0, 0.25, 0.5, 1, 2) respectively. 800 μL of supernatant was membrane filtered (30 kDa) in 4 vials for 5 washes and resuspended in equal volumes of DI water between each wash. Total volume samples of 300 μL at concentration of 25.0 ± 3.0 μg/mL had varying ratio DNA added followed by 30 min bath sonication (Fisher Scientific Ultrasonic Bath). Samples were tested at reference pH using NS3 NanoSpectralyzer then altered to pH 12 ± 0.25 using small aliquots of NaOH (≤ 3.0 μL), then tested again using NS3 NanoSpectralyzer.

Additional 1 mL dispersion mixture using $(GT)_{20}$ (2mg DNA, 1mg SWCNTs) in DI water with 0.1 M NaCl and pH 12 was prepared. pH was raised using small aliquots of NaOH and tested in Mettler-Toledo table-top pH meter. SWCNT-DNA mixture was tip sonicated in ice bath for 2 hours at 8 W. After centrifugation at 17000g for 90 min at 20 ± 2 °C, the supernatant of DNA-wrapped SWCNTs was collected and tested at 20x dilution using NS3 NanoSpectralyzer in 1cm path length quartz cuvettes.

The supernatant for DNA-SWCNT dispersion for each $(GT)_n$ was used to perform ATP separation at 20 ± 2 °C using wide range pH (1-13). 45 μL supernatant and 105μL PEG/DX (5.50% PEG / 7.50% DX) mixture prepared and pH altered using small aliquots of HCl and NaOH (≤ 3.0 μL) then vortexed. Mixture pH tested using Mettler Toledo table-top pH meter with ± 0.25 variance from target. PVP added in increasing increments with intermittent vortexing until SWCNT distribution into the PEG-rich top phase is visually evident, then centrifuged the sample for 3 min at 17000g. Top-phase separation tested using NS3 NanoSpectralyzer at 10x dilution in DI with an equal proportion reference of blank PEG/DX top phase in DI.

The supernatant for DNA-SWCNT dispersion for each $(GT)_n$ was diluted 20-fold in DI and NaCl to a resulting 100 mM NaCl concentration. Small aliquots of NaOH (≤ 3.0 μL) and HCl (≤ 3.0 μL) were utilized to adjust pH conditions to acidic (pH=2.0 ± 0.25) and alkaline (pH = 12 ± 0.25). Supernatant was tested for absorbance and NIR fluorescence using NS3.

3 Results and Discussion

3.1 $(GT)_6$-wrapped SWCNT Dispersion at Second Deprotonation pH of Guanine

SWCNTs require dispersal in order to overcome their insolubility and be converted into a functional colloidal medium that reduces aggregated bundles and impurities. The dispersion of SWCNTs allows for optimal surface interaction with the surrounding solvent and the separation of single chirality species required for future application in bioimaging and biosensing. For this article, DNA oligomers act as the dispersant by wrapping around the SWCNT.[19,22,46,61] Traditionally, DNA-wrapped SWCNTs are dispersed at solvent pH, in this case deionized water. After determining the increased optical properties at pH 12 due to second deprotonation of guanine and oxidation reduction, dispersion of SWCNTs at pH 12 was conducted to investigate the effects on dispersion quality and yield.[24,58]

Two dispersions were conducted using $(GT)_6$ at solvent pH of 5.99 and at a controlled pH of 11.95. After tip sonication process, the controlled pH is reduced from 11.95 to 9.96. The supernatants were diluted 20 times and tested using the NS3 NanoSpectralyzer for optical characterization. The absorbance and fluorescence spectrum of the solvent pH dispersion was first tested after tip sonication, then had the pH raised to 9.83 and tested again as a reference against alkaline dispersion. Minimal drop in absorbance is seen due to the addition of NaOH at this step. Absorbance results for solvent pH show a high enrichment of (6,5) species SWCNTs (~995 nm) with negligible enrichment of other species. After the solvent pH dispersion was raised to 9.83 an increase in large diameter tubes was evident. The (7,5) (E_{11} ~1040 nm) and (7,6) (E_{11} ~1140 nm) species showed high enrichment along with the (6,5) species, which is due to the reduction

of oxidation in alkaline conditions.[58] The controlled pH dispersion resulted in an even greater abundance of large diameter SWCNTs (Figure 3.1).

Additionally, fluorescence data depicts increased shielding of all three enrichment peaks. The quality and yield of pH-controlled dispersion is evidently higher than that of a dispersion conducted at solvent pH, and pH alteration after dispersion is unable to reach similar values. (8,4) species nanotubes see a 2x increase from absorbance values of 0.53 in solvent pH to 0.92 in alkaline conditions (Figure 3.3). The fluorescence of nanotube species dispersed in alkaline conditions show an emission increase ranging from 4 to 13 times, (6,5) and (7,5) respectively, then that of species dispersed at solvent pH. By altering the pH before dispersion to the second deprotonation level for guanine, the increased electrostatic forces are allowing for increased π-stacking of nucleobase-nucleobase and nucleobase-nanotube.[25,41] The density of DNA on SWCNT surface is higher due to tighter folding allowing for more DNA to adsorb to surface (Figure 3.3). Additionally, a greater reduction of oxidation potential is seen from the high level of large diameter tubes dispersed.

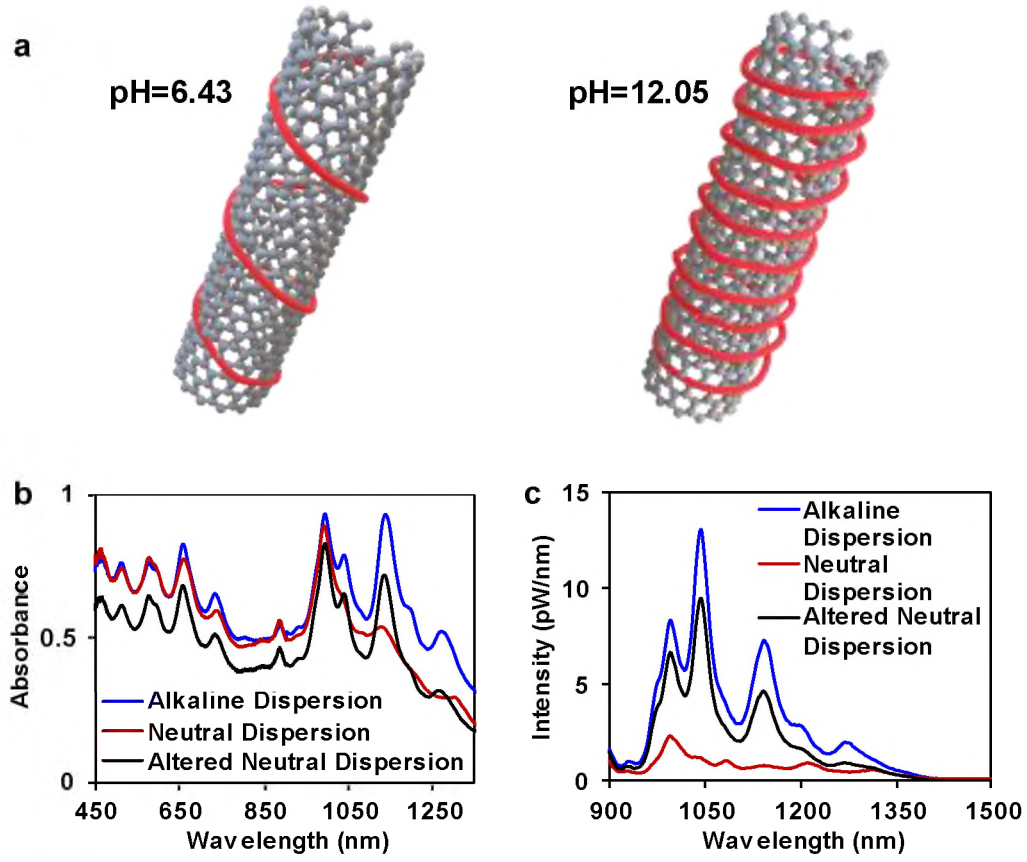

Figure 3.1: (a) Schematic of increased DNA wrapping structure at second deprotonation pH for guanine nucleobase as a result of increased π-π stacking between nucleobase-nucleobase and nucleobase-SWCNT. (b) Absorbance spectra displaying increased quality and yield of alkaline dispersion and reduction of oxidation potential shielding large diameter nanotubes. (c) NIR fluorescence displaying elevated emission intensity as a result of increased electron shielding from the quenching solvent

3.2 Correlation of ssDNA length on Optical Properties and Dispersion Yield for SWCNTs

Single-stranded DNA has been studied extensively for dispersion of SWCNTs due to the resulting high dispersion yield and biocompatible nature. The intrinsic biocompatibility of DNA and unique fluorescent properties of SWCNTs make the hybrid DNA-wrapped SWCNTs ideal for biosensing and bioimaging.[7,8,12] Further research on

solvent conditions and length distribution can be used to optimize optical characterizations at lower SWCNT concentrations.[62,63] Initial determination of research began with selection of ssDNA to utilize for dispersion of SWCNTs that would show controlled pH dependency.

$(GT)_n$ (n=6,10,15,20) was chosen based on presence of the guanine nucleobase, which shows unique first and second deprotonation, at pKa=9.19-10.03 and >11.94 respectively, and high yield dispersion capabilities (Figure 7.1).[41,59,63] Initial dispersions for each oligomer length were diluted 20x in deionized water to collect emission at 532 nm excitation and absorbance data. Shortest oligomer length, $(GT)_6$, showed elevated fluorescence (~ 30 pW/nm) at 995 nm and increased yield when compared to additional lengths (Figure 3.2). This is due to shorter sequences binding to SWCNTs with a higher density; therefore, increasing the electron shielding from the quenching solvent.[63] Subsequent oligomer lengths showed negligible emission changes. Absorbance study was inconclusive as to whether dispersion yield increased as oligomer length decreased, or if after a particular length is reached dispersion and emission qualities become constant.

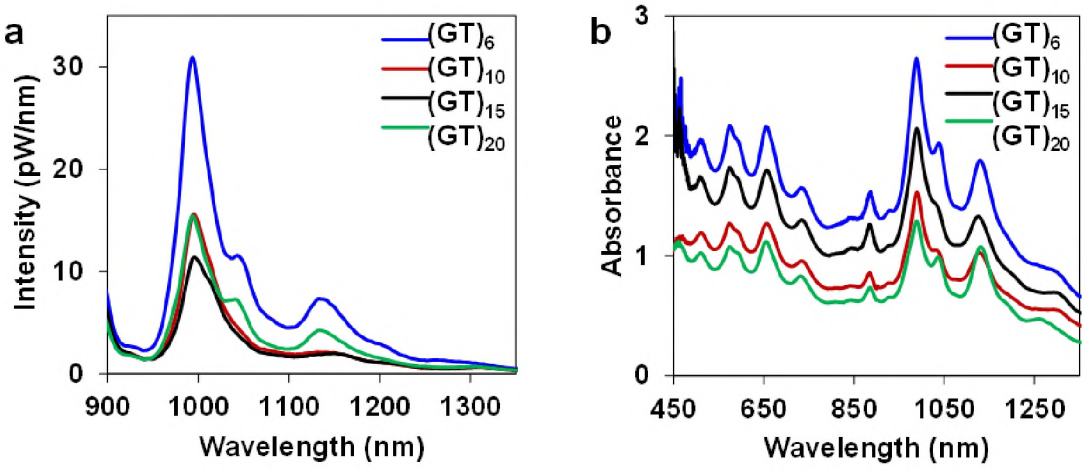

Figure 3.2: Varied $(GT)_n$ oligomer length show (a) $(GT)_6$ showing 2-fold emission values for (6,5) species nanotubes signifying higher DNA concentration on nanotube surface shielding electrons from quenching solvent and (b) shorter oligomer length results in increased quality and yield of DNA-wrapped SWCNT dispersion.

3.3 Optical Characterization of $(GT)_n$-SWCNT hybrids at Controlled pH

Initial inquiry into this study required the determination of nucleobase deprotonation utilizing absorbance and NIR fluorescence spectrum of DNA-wrapped single-wall carbon nanotubes. Guanine was chosen as the focal nucleobase due to the two unique deprotonation levels. Guanine displays first deprotonation at pKa = 9.19-10.03 and second deprotonation at pKa > 11.94 (Figure 7.1).[59] Using the $(GT)_n$ (n = 6, 10, 15, 20) oligomer, CG100 SWCNTs were dispersed and diluted to 20.0 μg/mL ± 2.0 μg/mL using the extinction coefficient 0.0416 L mg^{-1} cm^{-1}.[60] Initial dilution of supernatants resulted in a pH of 6 ± 0.5 and was used as the reference spectrum for each sequence. The optical characterization was studied at wide range pH (1-13) to determine the deprotonation effects of guanine on SWCNTs.

Absorbance patterns of $(GT)_6$-SWCNTs show acidic conditions (pH 1-6) favoring shorter wavelength nanotubes (~995 nm); however, as alkaline levels increased,

absorbance values at larger wavelengths increased exponentially. Additionally, NIR emissions at excitation 532 nm show a slight increase beginning at pH 7 and leveling at pH 9, which then steeply increases from pH 10-12 with pH 12 being the pinnacle (Figure 3.3). Larger wavelength SWCNTs (~1140 nm) show a larger increase in comparison to shorter wavelength (~995 nm) SWCNTs. These results coincide with the first deprotonation and second deprotonation of guanine. The results show a combination of two phenomena occurring with increased alkalinity.

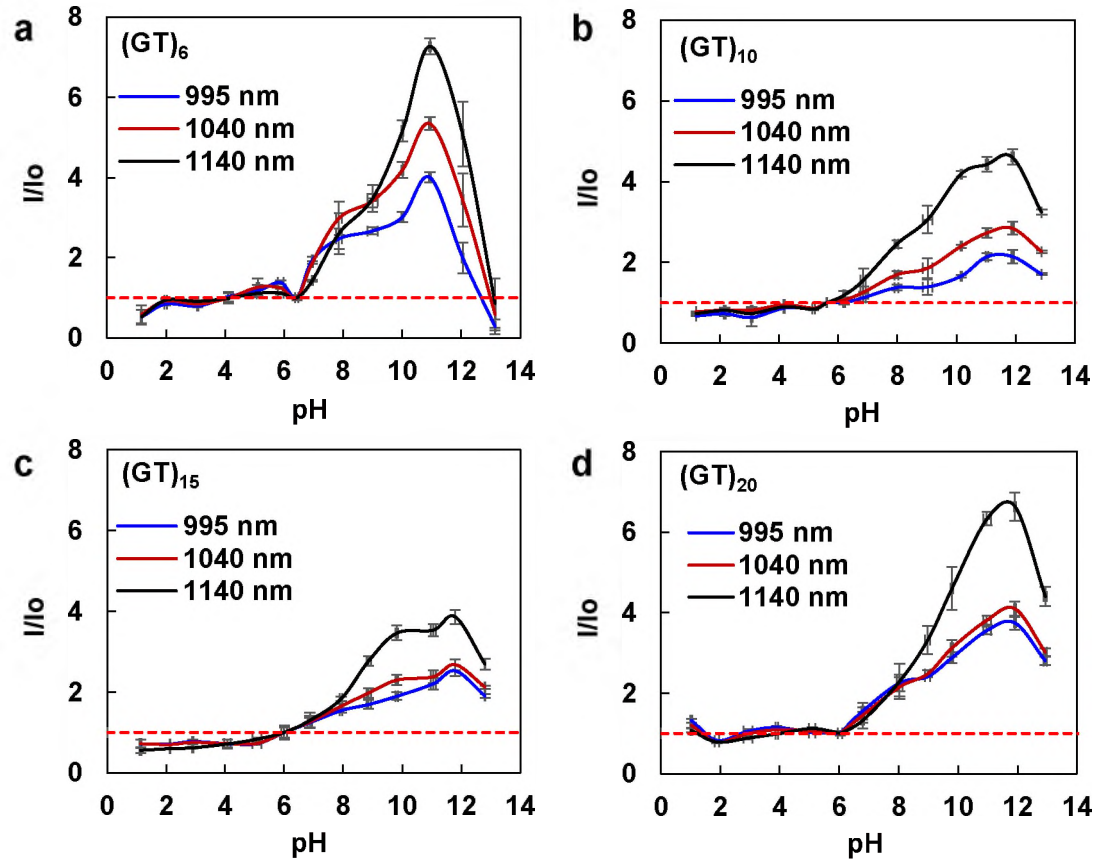

Figure 3.3: A significant increase of fluorescence emission can be seen in 2 elevations, initially with the first deprotonation pKa of guanine (9.19-10.03) and next with the second deprotonation pKa of guanine (>11.94) for (a) $(GT)_6$, (b) $(GT)_{10}$, (c) $(GT)_{15}$, and (d) $(GT)_{20}$ dispersed SWCNTs with large diameter tubes showing constructive amplification caused by both deprotonation and reduction of oxidation potential

Firstly, all significant SWCNT enrichment peaks are increasing with the first deprotonation and second deprotonation of guanine due to increased shielding of DNA on the SWCNT reducing the ability of solvent to quench electrons.[64] Additionally, larger wavelength nanotubes show high sensitivity to the increased alkaline levels due to the proclivity for oxidation. The high oxidation potential for large diameter nanotubes is reduced by the increased alkalinity resulting in a two-fold increase of absorbance and fluorescence when paired with the deprotonation shielding.[58] Additional $(GT)_n$ sequences were tested and showed similar patterns to $(GT)_6$ (Figure 3.3).

3.4 Effects of Free DNA Addition to DNA-wrapped SWCNT hybrids at Second Deprotonation pH for Guanine

The Second deprotonation of guanine (pKa > 11.94) resulted in the maximum increase of optical properties on $(GT)_n$-wrapped single-walled carbon nanotubes due to increased shielding from the electron quenching solvent.[59] In order to determine the causation of increased shielding, $(GT)_6$-wrapped SWCNTs were studied with variable amounts of free DNA during pH alterations. The SWCNT:DNA mass ratio from 1:n (n = 0, 0.25, 0.5, 1, 2) was carried out to determine if increased shielding was a direct result of additional free DNA wrapping on the SWCNT surface at pH 12 ± 0.25. If additional DNA began wrapping on the surface, results would show increases in intensity as free DNA concentration increased in till surface coverage reached a saturation point. However, no significant increase in intensity values was shown to correlate with increased concentrations of free DNA; therefore, increased electron shielding must be a direct result of conformation changes on the DNA already present on the surface on the SWCNT.

Shorter diameter nanotubes, signified by the E_{11} peaks at 995 and 1040 nm, showed a 2-3-fold increase in emission, while showing minimal changes in absorbance. The larger diameter nanotubes, signified by the E_{11} peak at 1140 nm, showed an approximate 5-fold increase in emission and 2-fold increase in absorbance (Figure 3.4). This is due to the reduction of oxidation from alkaline conditions.[58] Therefore, the deprotonation of the guanine nucleobases is increasing the π-stacking occurring between the nucleobases, guanine and thymine, drawing them closer together to form a tighter wrapping structure on the nanotube.[25] The increased π-stacking directly increases the hydrogen bonding occurring between nucleobases as a result of increased electrostatic forces.[25] The second deprotonated guanine, lacking two hydrogen atoms, forms stronger hydrogen bonds with neighboring nucleobases drawing the nucleobases closer together and in turn forming a tighter folding structure on the nanotube surface.

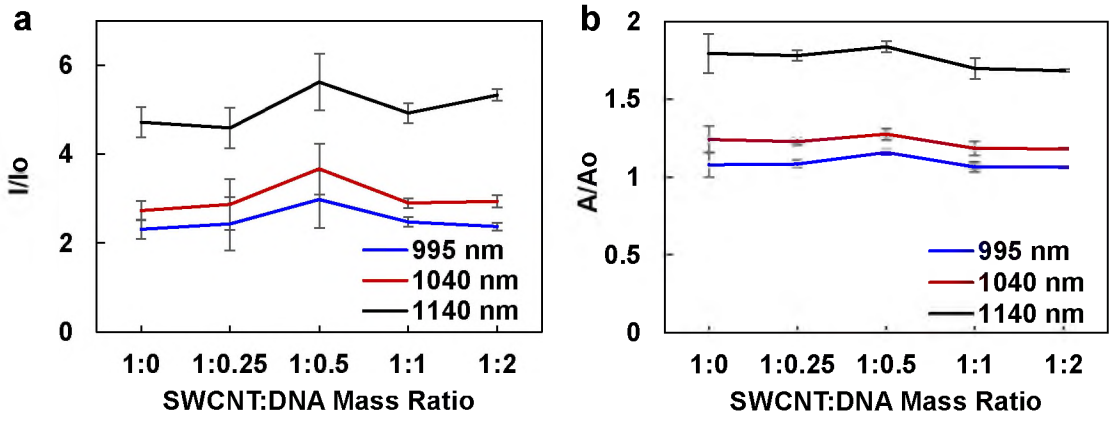

Figure 3.4: (GT)6-wrapped SWCNTs at pH 12 ± 0.25 with varying mass ratios of SWCNTs to DNA for (a) dimensionless fluorescence intensity at 641 nm excitation and (b) dimensionless absorbance display no increase in electron shielding from the electron quenching solvent signifying no additional DNA wrapping after dispersion.

3.5 Aqueous Two-Phase Separations in Controlled pH Conditions

Aqueous two-phase (ATP) separation has been studied extensively as a method of separating single-chirality SWCNTs.[19,22] The ATP extraction method functions based on a phase separation between two polymers which are immiscible with one another. This immiscibility is caused by the difference in solvation energies and therefore difference of hydrophobicity.[61,65] In this research, we are utilizing the hydrophilic polymer DX and the hydrophobic polymer PEG. The substantial gap between each polymer's solvation energy requires the use of PVP to act as a mediator and modify the DNA-wrapped SWCNTs to cross the phase separation. Without PVP, all of the DNA-wrapped SWCNTs used here would lie in the hydrophilic DX phase, but by adding increasing amounts of PVP we are able to close the gap between solvation energies and transition single-chirality species into the hydrophobic PEG phase.

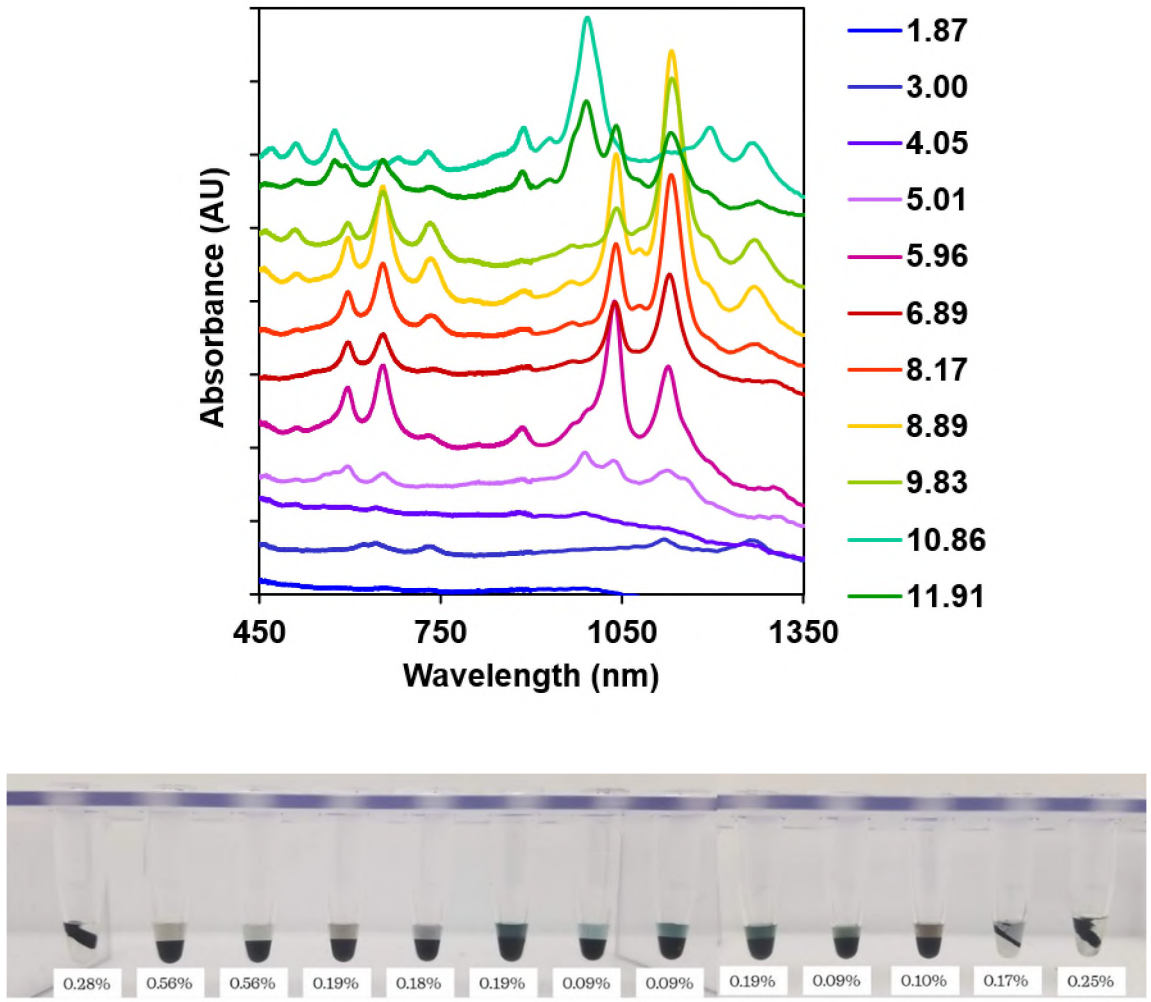

Figure 3.5: Aqueous two-phase extraction on (GT)15-wrapped SWCNTs via PEG/DX polymer system at wide range pH 1-13 (left to right) with corresponding % of PVP added

Additionally, this research is studying the modulation of DNA-SWCNT separation through the alteration of solvent pH. The addition of NaOH is raising the pH and slowly increasing the hydrophobicity of the DNA-wrapped SWCNTs.[21,66] At different alkaline levels, the hydrophobicity of the species is altered, which in turn allows for different species to be separated during ATP separation. The $(GT)_{15}$ wrapped SWCNT shows how one ssDNA sequence can be used to separate different species of SWCNTs at different pH

levels. Additional separation data for $(GT)_n$ and separation specifics can be found in (Figure 7.2 and Figure 7.3)

Acidic conditions (pH 1-5) resulted in no separation of singular species after addition of PVP; however, from pH 5.96 to 8.89 we begin two see two enriched species peaks at 1042 nm and 1142 nm characteristic of (7,5) and (7,6) species respectively (Figure 3.5). At pH 5.96, the (7,5) species is slightly favored for separation; however, as pH reaches more alkaline levels favorability is transferred to separation of the (7,6) species. At pH 9.83 singular (7,6) enrichment E_{11} can be seen; however, as pH exceeds 10, the (7,6) species is no longer seen in separations. At pH 11.91 a strong (6,5) E_{11} peak can be seen, but due to the broad nature of the peak there are likely large amounts of impurities present.

4 Conclusion

In summary, we have demonstrated how alterations to pH levels can be utilized to increase π-stacking between nucleobase-nucleobase and nucleobase-nanotube depending on deprotonation characteristics of the nucleobases present on ssDNA and at what step pH is optimized. The deprotonation of DNA nucleobases after dispersion at solvent conditions allows for tighter folding structure due to the increased electrostatic forces, hydrogen-bonding, and π-stacking, which in turn exponentially increases the fluorescent emissions up to 7-fold through electron shielding. The deprotonation of DNA nucleobases before dispersion allows for increased DNA wrapping and increases in fluorescent emissions up to 13-fold due to elevated electron shielding and reduction of oxidation potential resulting in a higher quality dispersion. The alkaline conditions also reduce oxidation potential of large diameter SWCNTs and in turn increase their fluorescent emissions roughly double that of smaller diameter tubes. The increased fluorescent emissions show promise for

bioimaging and biosensing, because it will allow for reduced concentrations of SWCNTs to be introduced to biological samples but still produce the required fluorescence. Also, the addition of NaOH to DNA-SWCNTs alter the hydrophobicity allowing for different species to be separated at different pHs using aqueous two-phase extraction.

CHAPTER IV

CARBOHYDRATE-PROTEIN BINDING INTERACTIONS USING NONCOVALENT COMPLEXES OF GLYCOPOLYMER-WRAPPED SINGLE-WALL CARBON NANOTUBES

1 Introduction

Single-wall carbon nanotubes (SWCNTs) have unique optical, electronic, and chemical properties which can be utilized for a wide range of applications, such as biosensing and imaging advancement in the near-infrared spectral range.[1–5,7,10,11,28] These applications are facilitated *via* stable dispersion of SWCNTs by biopolymers in an aqueous environment. Biopolymers allow for polymer backbones to be functionalized with biological entities that play vital roles in the function of living systems. Living systems require elaborate molecular recognitions sequences through carbohydrate-protein, protein-protein, and antigen-antibody interactions to function properly and these interactions occur via hydrophobic and electrostatic interactions and hydrogen bonding.[26] Carbohydrates of the cell membrane (glycans, glycolipids, etc.) play a vital role in a multitude of cellular events, such as cell-cell adhesion, cancer metastasis, and intracellular communication.[14,26–

[28] The carbohydrate covered cell surface is referred to as the glycocalyx.[27] On bacterial cells, the glycocalyx is responsible for avoiding immune cell recognition and adhering to the host cells making these carbohydrate-protein interactions the primary method of bacterial attachment to human cells.[27] Often times, viral and bacterial cells will attach via a carbohydrate-binding protein (lectin) to the glycocalyx of the human cells which is why a further understanding of the carbohydrate-lectin interactions is imperative to develop a future in the biosensing and imaging of pathogens and biopharmaceuticals.[26,27] Lectins can be found in plants, animals, bacteria, and viruses.

Lectin interactions are comprised of a series of weak molecular interactions, hydrophobic and electrostatic forces and hydrogen bonding; however, these interactions accumulate to become a strong force when the lectin displays multivalent interactions.[26] Lectins displaying binding affinity with monovalent carbohydrate ligands are significantly weaker with dissociation constants (K_D) in the 1-0.1 mM range compared to multivalent carbohydrates on the nM scale.[27] The focus on multivalent interactions has made synthetic glycopolymers (i.e., polymers with carbohydrate pendant groups) a focal point of study for understanding carbohydrate-lectin interactions due to their capability of mimicking natural glycoconjugates. Additionally, synthetic glycopolymers are tunable, meaning they can be synthesized with high sugar density thereby increasing access to multiple binding sites on proteins. Also, synthetic glycopolymers can be synthesized to be linear or hyperbranched to alter the crosslinking and binding conformations between lectins. The ability of a glycopolymer to successfully bind with multivalency to a protein is dependent on numerous properties, such as polymer length, sugar density, saccharide composition, flexibility, and conformation.[14]

Lectins binding to the glycoproteins and glycolipids of the glycocalyx in animals and plants can result in cross-linked complexes on the cellular surface. These cross-linked complexes play a vital role in biological responses, such as mitogenic activities and bulk transport.[29] Through the multivalent interactions, homogeneous cross-linked lattices begin to form between the specific recognition pair of carbohydrate-lectin regardless of the presence of other molecules. This allows for cross-linked lattices to precipitate the binding pair, shown in studies involving *Concanavalin A* with mannose/glucose specific glycoproteins.[29] Synthetic glycopolymers should be able to mimic the biomolecules and substitute into the cross-linked lattice for their specified carbohydrate-binding protein.

In this work, we study the behavior of synthetic glycopolymers and their ability to stabilize SWCNTs *via* noncovalent complexation resulting in water soluble, glycopolymer-wrapped SWCNT (Glyco-SWCNT) hybrids. Particularly, disaccharide lactose-containing polymers of various chain lengths will be tested to optimize dispersion stability, quality, and yield of SWCNTs. These Glyco-SWCNT complexes will be utilized to explore the mono- and multivalent interactions between carbohydrates and various lectins *via* optical spectroscopy with the goal of determining the selectivity and sensitivity of targeted interactions between carbohydrates and proteins. The Glyco-SWCNT complexes will be tested to see if they can mimic the role of the glycocalyx in cross-linked lattices with carbohydrate recognition lectins. Additionally, FITC-marked lectins will be utilized to determine kinetic parameters for various lectins as they interact with the glycopolymer surface. If successful, these Glyco-SWCNT complexes can be utilized as fluorescent probes to detect specific carbohydrate-protein interactions in biology that are important for many cellular events, such as cancer development and metastasis.

2 Materials and Methods

Lactose homopolymers of chain length 400 and 415 were synthesized using cyanoxyl free radical-mediated polymerization (CFRMP) scheme.[60] CoMoCAT SWCNT powder (SG65i-L39, Chasm Advanced Materials) was dispersed using Lact-AM 415 by tip sonication (model VCX 130, Sonics and Materials, Inc.) in an ice bath for a total of n minutes (n= 40, 30 + 30, 45 + 45, 40 + 40 + 40, and 120 with + indicating 30-minute rest). A total dispersion volume of 1 mL was comprised of 0.1 mg SWCNT and 0.4 Lact-AM 415 in deionized water (DI). After tip sonication, dispersion was separated into 9 samples of ~100 μL that were then centrifuged at 17,000 g and 19 °C for 90 minutes to collect supernatant. Absorbance and NIR fluorescent data were gathered using the NS3 NanoSpectralyzer (Applied NanoFluorescence, LLC) to determine dispersion quality and yield.

CoMoCAT SWCNT powder was dispersed using Lact-AM 415 by tip sonication in an ice bath for a total of 45 + 45 minutes with a 30 minute rest period between. The SWCNT:glycopolymer mass ratio of 1:n (n=0.5, 1, 2, 3, 4, 8) was analyzed, with the SWCNT concentration being 0.1 mg/mL. Supernatant was collected by separating dispersion into 9 samples of ~100 μL and centrifuging at 17,000 g and 19 °C for 90 minutes. Absorbance and NIR fluorescent data was gathered using the NS3 NanoSpectralyzer to determine SWCNT concentration using the extinction coefficient 0.04163 L/mg·cm at 780 nm.[60]

CoMoCAT SWCNT powder was dispersed using Lact-AM 400 by tip sonication in an ice bath for a total of 45 + 45 minutes with a 30 minute rest period between. The

SWCNT:glycopolymer mass ratio of 1:4 was used for all lectin experimental procedures, with SWCNT concentration being 1 mg/mL. Supernatant was collected by separation dispersion into 9 samples of ~100 μL and centrifuging at 17,000 g and 19 °C for 90 minutes. Supernatant was diluted 9x in phosphate buffer solution (PBS) in preparation for lectin addition.

Arachis hypogaea (PNA), *Concanavalin A* (ConA), *Galanthus nivalis* (GNA), and Bovine serum albumin (BSA) were purchased from Sigma Aldrich. A mass ratio analysis on SWCNT:PNA using 1:n (n=0, 1, 2, 4, 8, 16) was conducted to determine optimal incubation time for lectin addition based on diminishing visible fluorescence peak of FITC marker at 525 nm after varied time increments. The optical spectroscopy characterization of glyco-SWCNTs including vis-NIR absorbance and fluorescence was measured using NS3 NanoSpectralyzer at 0 min, 5 min, and 10 min from PNA addition.

Competitive and sequential binding was carried out using Lact-AM 400 dispersed SG65i SWCNTs at 8x dilution in PBS. Competitive binding utilized adding 0.8 uM lectin (PNA/ConA) and 0.041 mg of free lactose to supernatant and incubating for 5 min before centrifuging 4 min at 17,000 g and 19 °C. Supernatant was collected and tested using NS3 NanoSpectralyzer. Sequence binding I was performed by adding 0.041 mg of lectin to the nanotube sample, incubating 5 min, then adding 0.8 uM lectin (PNA/ConA). The sample was then vortexed and incubated an additional 5 minutes before centrifugation and collection of supernatant as described for competitive binding. Lastly, sequence binding II was performed by first creating a solution of 0.041 mg of free lactose and 0.8 uM lectin (PNA/ConA) that was allowed to incubate 5 min. That solution was then added to Glyco-

SWCNT dilution and allowed to incubate 5 min before proceeding with previously described centrifugation and collection of supernatant.

Supernatant was diluted 8x in PBS and all lectins were added at n μM concentration (n= 0, 0.05, 0.1, 0.2, 0.4, 0.8, 1.5). Samples were incubated for 5 min after lectin addition then centrifuged for 3 min at 17,000 g and 19 °C to collect supernatant. Absorbance and NIR fluorescence were collected using the NS3 NanoSpectralyzer.

Additionally, sequential vis-fluorescence of the FITC marked PNA and ConA at concentration of 2.25 ± 0.1 μM concentration was conducted for 300 s at 5 s intervals using NS3 NanoSpectralyzer. Assuming the model for a a pseudo first-order reaction, a rate constant (k_A), kinetic coefficient (A), and correction factor (B) were found using the following equation:[14,27,47,67]

$$\frac{I(t)}{I_0} = A(1 - e^{-k_A t}) + B \qquad [1]$$

where I_0 and I are fluorescence intensity of FITC at 525 nm wavelength before and after lectin addition.

3 Results and Discussion

3.1 Noncovalent Glyco-SWCNT Complexes

Glycopolymer dispersed SWCNTs have warranted tremendous attention recently due to the ability for synthetic glycopolymers to mimic the cell surface glycocalyx while incorporating the unique optical properties of the semiconducting SWCNT.[14,27,47,67] This affords a bright future for the investigation of cellular events through bioimaging and biosensing. Glycopolymers adsorb to the SWCNT surface via hydrophobic interactions with displayed stability.[67] The stability of Glyco-SWCNT hybrid dispersions is strongly

dependent on carbohydrate identity and polymer chain length.[47] Glycopolymers with branched monosaccharides showed significantly reduced dispersion yield when compared to glycopolymers branched with the disaccharide lactose. This is theorized to be due to disaccharides limiting polymer backbone flexibility in a manner favorable to the conformational angle needed for wrapping the SWCNTs while concurrently allowing for multivalent hydrophobic interactions to strengthen the forces.[47]

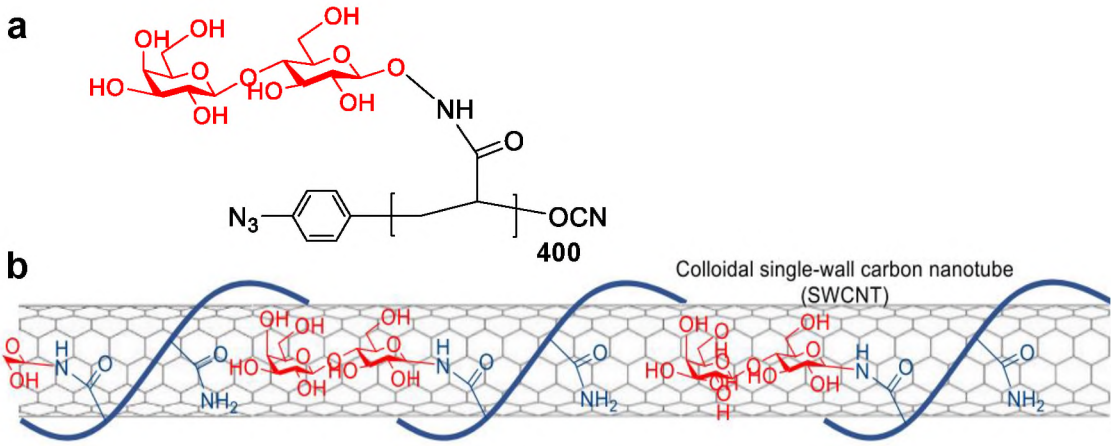

Figure 4.1: Schematic depicting (a) chemical structure of Lact-AM 400 and (b) theoretical wrapping structure of Lact-AM 400 on SWCNT surface. (Referenced by [46]).

In this work, we utilized disaccharide lactose-containing homopolymer with an acrylamide polymer chain length of n = 400 and 415 (i.e., Lact-AM 400 and Lact-AM 415 to disperse SWCNTs (Figure 4.1). Both dispersions showed excellent stability with Lact-AM 415 displaying an increased yield and quality (Figure 8.4). Initial tip sonication optimization results showed Glyco-SWCNT concentrations reaching 39.9 mg/L corresponding to a 39.9% nanotube dispersion yield for Lact-AM 415 and 36.38 mg/L corresponding to a 36.4% nanotube dispersion yield for Lact-AM 400 (Figure 4.2 and

Figure 8.4). This proves that glycopolymer dispersion capability is not only dependent on carbohydrate content, but also highly dependent on polymer backbone length. Transmission electron microscopy (TEM) shows efficient dispersal of isolated SWCNTs and the excess unbound glycopolymers form independent globular micelles within the supernatant (Figure 4.2). The E_{11} absorbance peak for the (6,5) species is clear at 1006 nm, displaying a red shift from the characterized 976 nm peak caused by the noncovalent functionalization of the glycopolymers.[16] Additionally, slight variations in diameter along the nanotube surface seen in TEM images display the varied glycopolymer content adsorbing to the SWCNT surface (Figure 4.2). The synthetic glycopolymers also display protective shielding of the SWCNT electrons allowing for their unique fluorescent signature to be used for future bio-application.

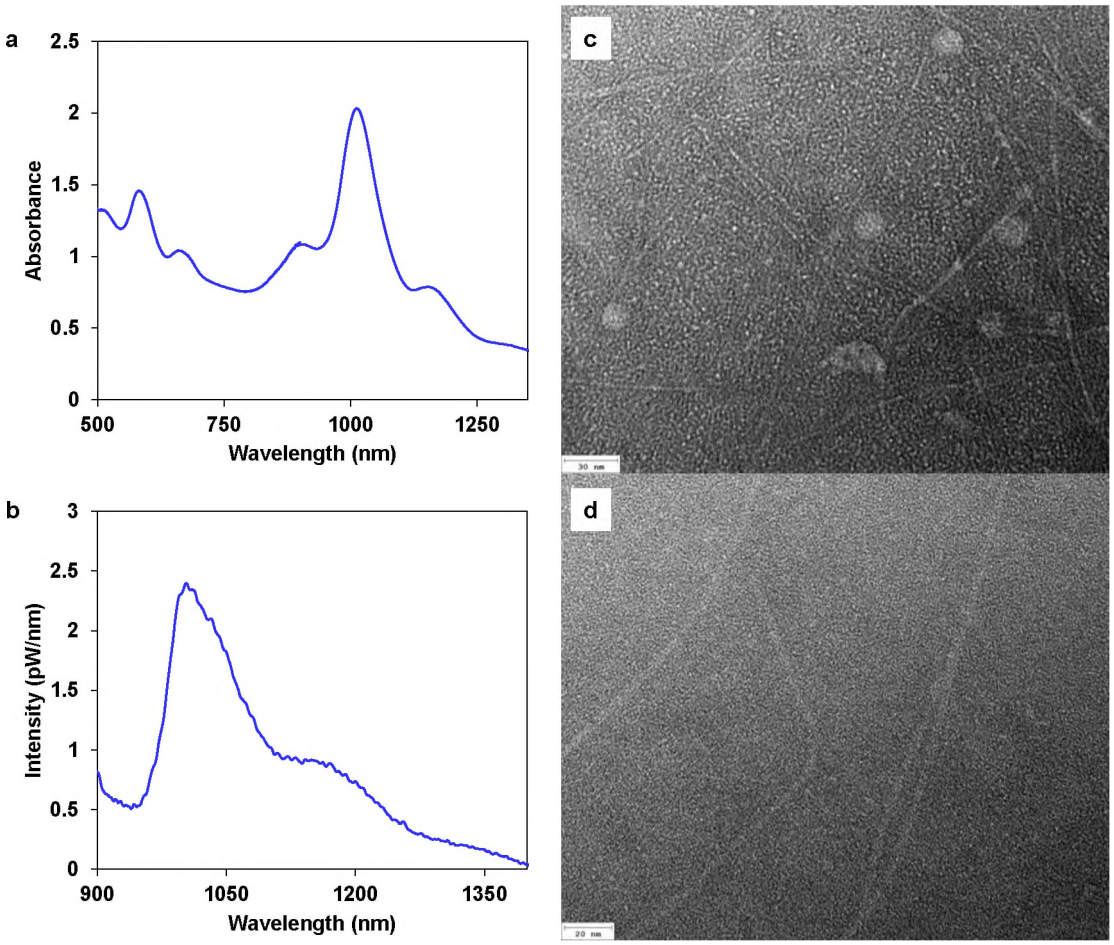

Figure 4.2: Glyco-SWCNT hybrid dispersion of (6,5) enriched raw SWCNT powder with disaccharide lactose-containing homopolymer. Lact-AM 400 shows efficient dispersal of SWCNTs through (a) enriched 1013 nm E_{11} peak in absorbance spectrum and (b) protected NIR photoluminescence of the SWCNTs. TEM images depict (c) uniform distribution of Glyco-SWCNTs hybrids in solvent conditions with free glycopolymer micelles forming due to excess Lact-AM 415, while (d) closer magnification displays slight diameter variation along nanotube signifying varied Lact-AM 415 concentration adsorbed on nanotube surface.

Additionally, there seems to be a correlation between the length of Lact-AM and the diameter of SWCNT favored in dispersion. Lact-AM 400 and 415 efficiently dispersed (6,5) enriched raw SWCNT powder but were inefficient in dispersing (7,6) enriched raw SWCNT powder (Figure 8.4). Shorter length disaccharide lactose-containing homopolymers were explored but proved incapable of efficient dispersion of the (7,6)

enriched raw SWCNT powder and future testing is required to determine the correlation between length and SWCNT diameter.

3.2 Glyco-SWCNT Complex Interaction with Varied Lectin Concentration

After optimizing Glyco-SWCNT dispersion techniques, we were able to focus on the main objective of exploring the carbohydrate-lectin binding interactions on the Glyco-SWCNT complex. Initial inquiry developed a catalogue of lectins (PNA, ConA, GNA, and BSA) to encompass both variable binding affinity and multivalency between the lactose present on the synthetic glycopolymers (Table 0II.1). Lactose is a disaccharide containing glucose and galactose. In choosing lectins we wanted to explore proteins with binding for each carbohydrate in addition to proteins with affinities to non-present carbohydrate.

Arachis hypogaea (PNA) has long been studied as a plant substitute lectin for researching human cellular response due to its ability to agglutinate neuraminidase-treated human red blood cells. This agglutination behavior directly mimicked the immunological response of anti-T antibodies of mammalian cells that occur in numerous bacterial and viral infections.[28,68] Additionally, *Concanavalin A* (ConA) is another plant lectin, derived from the jack bean, chosen due to its strong binding affinity for mannose and glucose, but also its nonbinding affinity towards galactose.[69] Both of these lectins exhibit multivalent binding sites; however, their difference in binding affinity can depict whether the galactose or glucose carbohydrate group of lactose is more readily available to bind. Whether the galactose or glucose carbohydrate binds more readily may shed light on the difference between terminal and internal carbohydrate interaction with SWCNT surface.

Lastly, two proteins were chosen that would show no binding affinity towards lactose, GNA and BSA. *Galanthus nivalis* (GNA), derived from snowdrop bulbs, shows a binding affinity for mannose, while Bovine serum albumin (BSA) is a protein with structural similarities to human serum albumin (HAS).[70] Both of these proteins were incorporated into this research to clarify that agglomeration occurring was in fact a result of cross-linking lattices forming between lectins and the bound Glyco-SWCNTs.

3.2.1 Cross-linked Lattice Agglomeration

Carbohydrate-lectin cross linking interactions has been widely documented and has an active role in apoptosis of activated human T-cells.[27,29] By gaining a more detailed understanding of this cross-linking phenomena, scientists can gain a deeper understanding of the interactions occurring between pathogenic lectins and the glycocalyx of human cells. The cross-linking lattices formed between lectins and carbohydrates have facilitated studies in quantitative precipitation of bound molecules and agglomeration studies on glycopolymer functionalized nanoparticles.[27,29]

In this research, we will be studying the aggregation of Glyco-SWCNT complexes caused by the phenomena of cross-linking between carbohydrates and lectins (Figure 4.3) using Lact-AM 400. Likewise, we have taken a closer look into the effects of binding affinity and multivalency on aggregation. Results show a strong correlation between terminal/internal carbohydrate placement and binding affinity to aggregation occurrence. Lectins with strong glucose binding affinity (ConA) show a greater tendency toward aggregation of the Glyco-SWCNT complexes, seen at 0.8 uM ConA resulting in 80% Glyco-SWCNT removal from the supernatant. Additionally, since pendant lactose attaches to the polymer backbone at the internal glucose group, lectins attached to the surface of

glucose to form cross-linking lattices would be more capable of pulling the adsorbed glycopolymer away from the nanotube surface. This further proves the ability for ConA to bind to internal carbohydrate groups due to it's extended binding site.[71,72] The pulling away of adsorbed glycopolymer may be responsible for the reduced number of Glyco-SWCNTs in the supernatant after incubation and centrifugation.

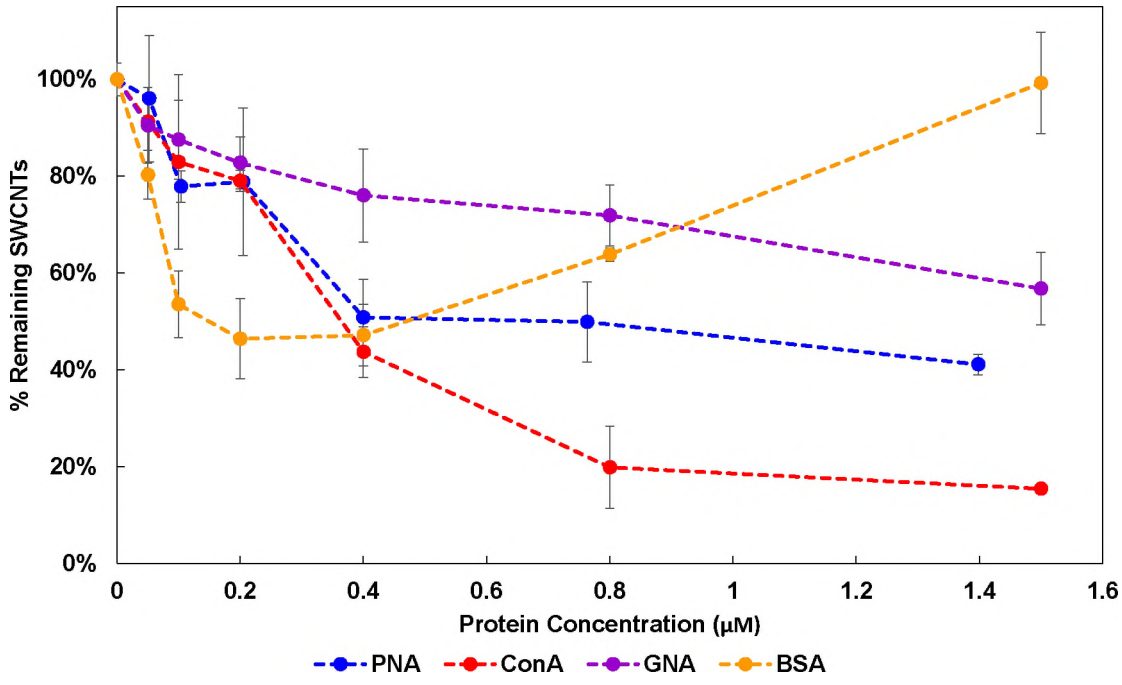

Figure 4.3: Agglomeration phenomena caused by cross-linking lattice formations between Glyco-SWCNTs hybrids and lectins studied at variable lectin concentration and subsequent agglomeration removal after incubation and centrifugation.

PNA displays a similar pattern of aggregation to ConA; however, after 0.4 μM PNA reaches binding saturation with 51% Glyco-SWCNTs remaining in the supernatant. This shows that lectins binding to glucose result in either a greater number of aggregations or more extensive glycopolymer removal from the SWCNT surface than galactose. This data supports that galactose is bound further from the SWCNT. Additionally, PNA's large

particle size (120,000 kDa) and tetramer structure may be hindering its ability to diffuse uniformly and quickly through the solvent. PNA reaches a maximum agglomeration effect here at 1.5 μM with 41% Glyco-SWCNTs remaining in the supernatant after incubation and centrifugation.

Lastly, GNA showed minimal aggregation over increased concentrations, which was expected due to GNA's primary binding affinity to the non-present mannose. At maximum agglomeration with 1.5 μM concentration of GNA, 57% of Glyco-SWCNTs remain in the supernatant. Additionally, BSA which does not display carbohydrate affinity, showed an unusual effect on the stability of Glyco-SWCNTs. At low concentrations of BSA (0.1 – 0.4 μM), Glyco-SWCNT stability in PBS was reduced resulting in 46-54% loss of Glyco-SWCNTs; however, at concentrations greater than 0.4 μM BSA stability began to increase. At 1.5 μM BSA, no significant loss of Glyco-SWCNTs occurs. This is most likely due to low concentration BSA diminishing Glyco-SWCNT stability due to its electrostatic forces.[73] The positively charged lysine groups of BSA began interacting with the SWCNT surface reducing the stability of Glyco-SWCNTs. At high concentrations of BSA, more BSA began adsorbing to the SWCNT surface, either replacing glycopolymer or adsorbing interstitially.[70,73] This resulted in the recovery of SWCNT stability.

3.2.2 Lectin Binding Effects on NIR Fluorescence

After determining the binding affinity of lectins for Lact-AM 400 functionalized SWCNTs (Figure 4.1), we wanted to determine how lectin binding would affect the SWCNTs fluorescent signatures. The unique fluorescent signatures of SWCNTs are imperative to the future application of Glyco-SWCNT complexes as biomarkers for pathogenic lectins. Results show that a depression of fluorescence is seen for all lectins

that showed binding affinity to Lact-AM 400 (Figure 4.4). This is theorized to be caused by the cross-linking between carbohydrates and lectins pulling the glycopolymers from the nanotube surface. With less glycopolymer surface coverage, solvent electron quenching diminishes the fluorescent intensity of the SWCNT. Interestingly, ConA showed a stronger fluorescence at 0.2 μM than PNA, 0.54 and 0.27 pW/nm respectively, even though at this concentration both lectins resulted in a loss of 21% Glyco-SWCNTs from the supernatant. This data further proves that glucose is more closely adsorbed to the SWCNT surface; therefore, ConA bound to the Glyco-SWCNT surface that has not formed cross-linking lattice structures would provide more shielding from the quenching solvent than the further bound PNA to glucose.

GNA showed minimal effects on NIR fluorescence, which is to be expected because it is not binding to any sugar group present on the Glyco-SWCNTs; therefore, there is no increased shielding from the quenching solvent nor is there glycopolymer being removed from the SWCNT surface. Meanwhile, BSA shows increased shielding of the SWCNT at concentrations greater than 0.4 μM. Fluorescent intensity reaches a maximum of 1.31 pW/nm from a starting intensity of 0.7 pW/nm. This further supports the argument that at high concentrations BSA is adsorbing to the SWCNT surface resulting in increased electron shielding.

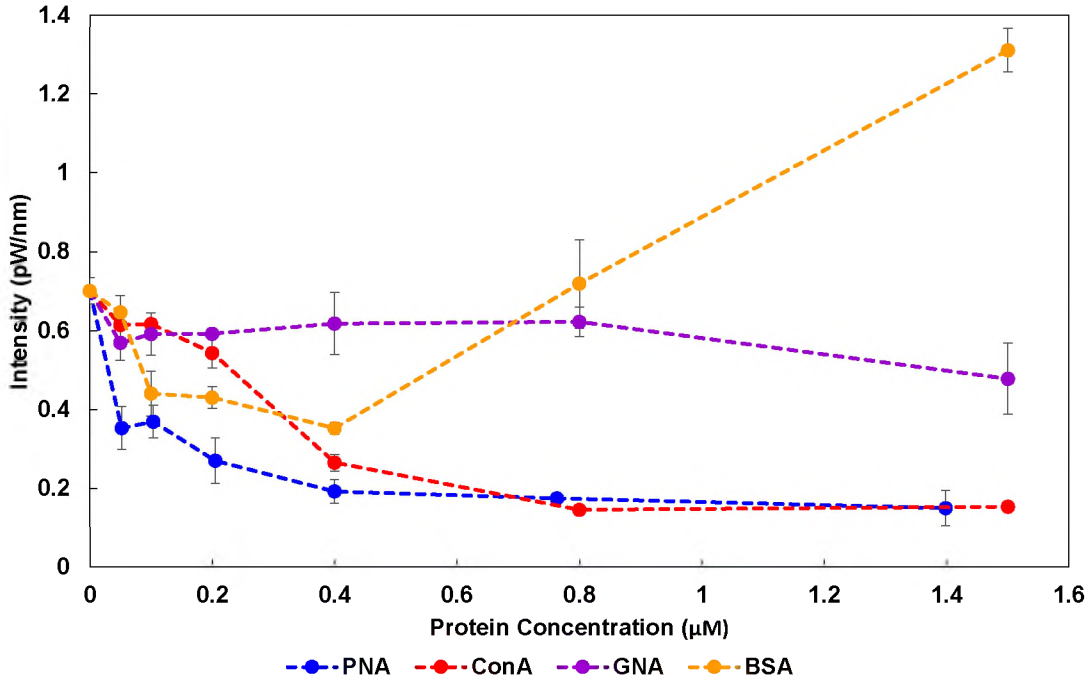

Figure 4.4: NIR fluorescent exploration of Glyco-SWCNT hybrids with varied lectin concentration after agglomeration removal via incubation and centrifugation depicts loss in emission for recognition binding lectins PNA and ConA and increased shielding at high concentrations of BSA due to surface adsorption.

3.3 Competitive and Sequential Binding of Glyco-SWCNT with Lectin

Synthetic glycopolymer have become an interest of study due to the ability to increase multivalent interactions between carbohydrate-lectin interactions due to the tunability of the pendant carbohydrates on the glycopolymer. To better understand the role multivalency plays in the Glyco-SWCNT complexes, we explored competitive and sequential binding. Absorbance data gathered using lectin concentration of 0.8 uM further shows increased aggregation caused by ConA. Additionally, PNA studies for competitive binding and sequence binding II show similar aggregation results of approximately 40-45% of SWCNTs removed when compared to lectin only binding. This displays that PNA favors binding to Glyco-SWCNTs complexes over that of free lactose, which would result

in no lattice formation aggregation. Sequence binding I resulted in an increased aggregation removal of approximately 77% likely due to free lactose interstitially binding to open sites on PNA where steric interferences between neighboring nanotubes block additional Glyco-SWCNT binding. This allows for increased hydrogen binding and tighter lattice formation structure. ConA showed elevated aggregation 80-91% SWCNT removal with competitive binding and sequence binding II displaying highest levels of aggregation.

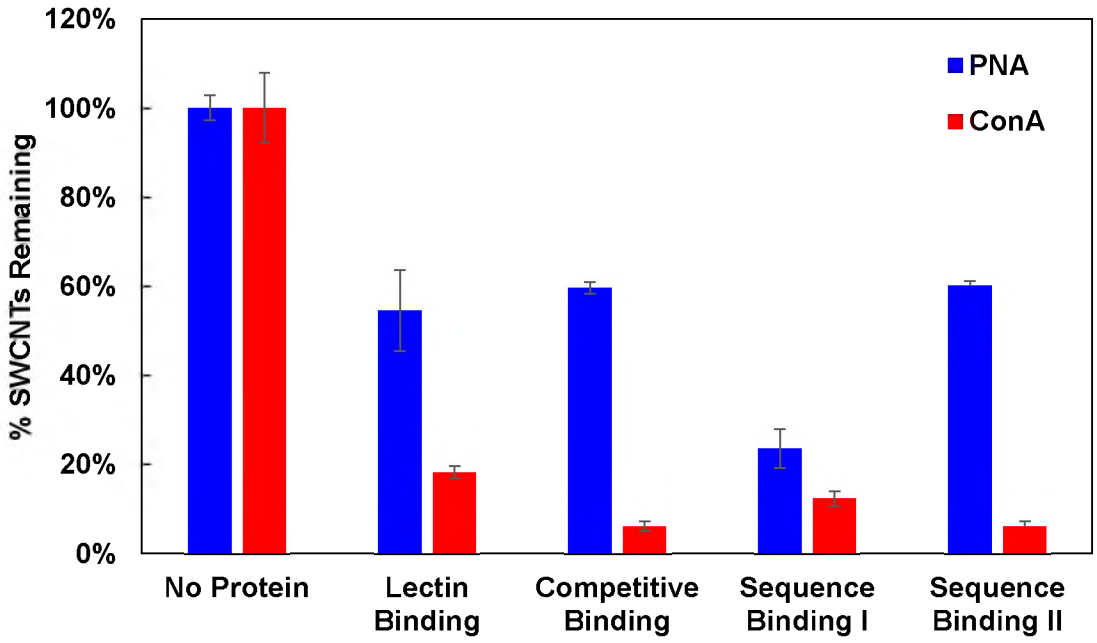

Figure 4.5: Agglomeration phenomena caused by cross-linking lattice formations between Glyco-SWCNTs hybrids and lectins studied using competitive and sequential binding with free lactose.

3.4 Glyco-SWCNT Lectin Interactions and Kinetic Parameters

FITC marked lectins undergo fluorescent quenching upon binding with a carbohydrate due to the fluorophore conjugated protein undergoing conformational changes.[12,54] Due to this fluorescent quenching, carbohydrate-lectin binding kinetics can be determined through the sequential acquisition of the Vis fluorescence after lectin is added (Figure 4.5). In this study, we analyzed the kinetic parameters of PNA and ConA binding at an excess concentration of 2.25 ± 0.2 μM to the Lact-AM 400 SWCNT complex. Assuming the reaction model for single-site surface adsorption (Equation 1), a kinetic parameter (k_A) kinetic coefficient (A), and a kinetic correction factor (B) were found for PNA and ConA (Table VIII.2). PNA has a time constant ($1/k_A$) of 38.42 ± 3.26 s, which is almost half that of ConA at 66.34 ± 3.62 s (Appendix B, Table VIII.2). Similarly, the kinetic coefficient for each lectin varies with -0.996 ± 0.066 and -0.702 ± 0.040 for PNA and ConA respectively. This shows that PNA reacts more quickly with galactose than ConA does with glucose. Both PNA and ConA are tetramer structures displaying multivalent interactions. We have previously shown that glucose is adsorbed more closely to the nanotube surface due to its attachment to the polymer backbone, while galactose is afforded more freedom towards the solvent. Theoretically, due to molecular structure of Lact-AM 400, it would make sense that the freer galactose molecule would react more readily with PNA than the sterically hindered ConA to glucose. In addition, control experiments show no binding interaction for DNA-SWCNT hybrids as seen in Figure 4.6.

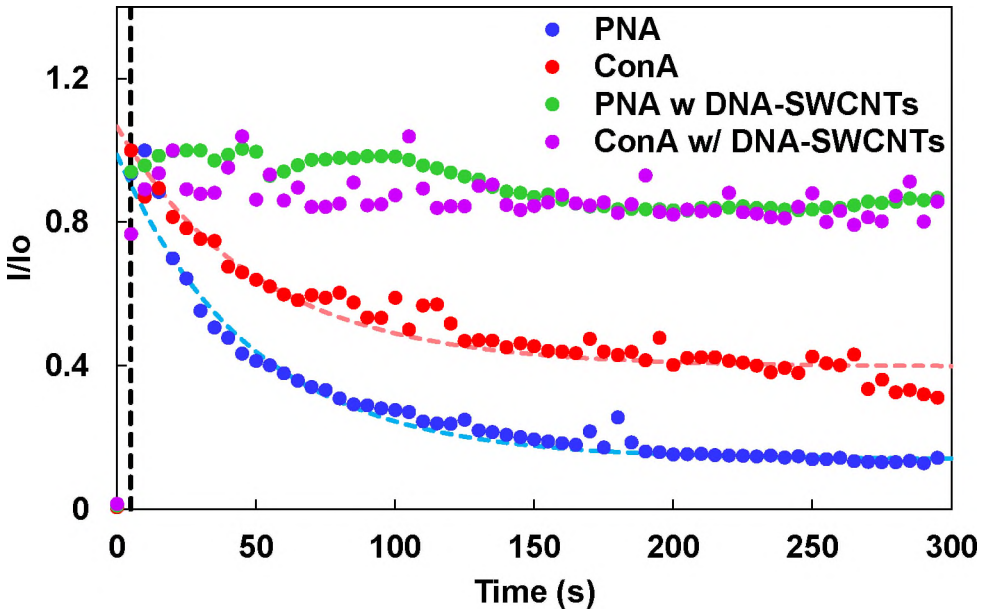

Figure 4.6: Sequence acquisition of dimensionless intensity illustrates the reaction rate of ConA and PNA when lectin is added at 5 seconds. Kinetic parameters were fit using single-site absorption model represented.

4 Conclusion

In summary, we have demonstrated that disaccharide lactose-containing homopolymers (Lact-AM 400 and Lact-AM 415) are efficient dispersants for (6,5) species SWCNTs while maintaining the SWCNT fluorescent signature. However, dispersion of different SWCNT species would require the development of a larger catalogue of glycopolymers to determine carbohydrate profile and polymer length required. Particularly, we investigated the ability of Glyco-SWCNT complexes to interact with recognition lectins as a precursor to the development of biomarkers designed to explore the carbohydrate-protein interactions occurring during cellular events. We studied the ability of lectins containing different carbohydrate binding affinities, structural conformations,

and multivalent sites to determine how protein binding to Glyco-SWCNT complexes would affect the intrinsic properties of the SWCNT.

Results showed aggregation caused by the cross-linking lattices between carbohydrates and lectins for Lact-AM 400 removed more glycopolymer from the SWCNT when bound to glucose over galactose. This is due to glucose being absorbed more closely to the nanotube surface. Galactose binding PNA showed decreased electron shielding at similar aggregation levels as glucose binding ConA, further supporting that glucose is bound closer to the nanotube surface than galactose. Together, these occurrences indicate that glucose is binding more closely to the SWCNT surface while the galactose molecule is more readily available for interactions. Likewise, kinetic data gathered for PNA indicates a faster binding reaction occurring than ConA. Since galactose is further from the nanotube surface, it is freer to react with PNA in the solution which explains the faster reaction rate. Overall, the process of carbohydrate-lectin binding utilizing Glyco-SWCNTs requires further investigation to optimize fluorescent signatures and expand glycopolymer-SWCNT recognition pairs to progress for future application as biosensors. However, this preliminary research shows a promising future utilizing Glyco-SWCNT complexes and helps to gain a further understanding of how lectins interact with the Glyco-SWCNT complex.

CHAPTER V

CONCLUSION

In conclusion, we have shown how the noncovalent complexation of single-wall carbon nanotubes with biopolymers has an extensive future of possibilities for designing nanosystems for numerous applications, from nanotube purification to biological sensors and bioimaging in nanomedicine. We have displayed the effects of solvent pH on optical characterization of DNA-wrapped SWCNTs due to the protonation/deprotonation of the guanine nucleobase to form additional tautomers at varied pKa. Additionally, we explored the effects of carbohydrate-proteins on Glyco-SWCNT complexes to determine protein binding kinetics and behavior.

The guanine nucleobase tautomer transformations at varied pKa values through the protonation, single deprotonation, and double deprotonation of the amine groups allows for DNA-wrapping conformation changes to exhibit elevated NIR fluorescent intensity up to 7-fold. Additionally, dispersions carried out at pH above the double deprotonation pKa value of 11.94 resulted in increased SWCNT quality and yield as well as NIR fluorescent intensity signifying additional DNA surface coverage on the nanotube. The different

protonation/deprotonation states of guanine tautomers exhibit changes in the DNA-wrapped SWCNT hydrophobicity displayed in the varied species enrichment of aqueous two-phase separation over wide range pH. This technique can be utilized to further separation quality and yield after additional research. Further work will explore the effect of varied nucleobase tautomers due to controlled pH for adenine, cytosine, and thymine. This will allow us to increase efficiency of biosensors at decreased SWCNT concentration as well as explore the possibility of DNA-wrapped SWCNTs as biomarkers for the imaging of pathogenic tissue displaying high acidity pockets, such as cancerous tumors.

Similarly, we have demonstrated how disaccharide lactose-containing homopolymers can effectively disperse SWCNTs while maintaining their fluorescent integrity allowing for the investigation of protein-carbohydrate interactions. Lactose attached to an acrylamide backbone at the glucose molecule shows binding capabilities for both galactose and glucose binding lectins, and aggregation could be seen for PNA and ConA signifying the cross-linking lattices formed between carbohydrate-proteins that is commonly found in pathogenic cellular surface events. PNA with galactose binding affinity showed faster reaction rates with a time constant of 38.42 ± 3.26 s, approximately half that of ConA at 66.34 ± 3.62 s. Competitive and sequential binding results showed that lectin will bind with Glyco-SWCNT complexes over free lactose due to high multivalency. Additionally, PNA displayed less glycopolymer removal from the surface of the nanotube, with 41% of Glyco-SWCNTs remaining after incubation and centrifugation. This is due to galactose being further from the SWCNT surface and more efficiently interacting with the solvent. Further work will include a more developed catalogue of lectin recognition for Glyco-SWCNT complexes as well as explore the

recognition between different glycopolymers and SWCNTs for efficient dispersal. This will allow for the progress of developing biosensors and bioimaging to investigation the cellular events related to pathogenic tissue.

REFERENCES

1. Dresselhaus, M. S., Dresselhaus, G. & Saito, R. Physics of carbon nanotubes. *Carbon* **33**, 883–891 (1995).

2. White, C. T. & Mintmire, J. W. Fundamental Properties of Single-wall Carbon Nanotubes. *Journal of Physical Chemistry B* 52–65 (2005) doi:10.1177/074193258901000304.

3. Shahzad, M. I., Tagliaferro, A. & Shahzad, M. I. Introduction to carbon materials. *Carbon for Sensing Devices* **9**, 3–14 (2015).

4. Bekyarova, E. *et al.* Electronic properties of single-walled carbon nanotube networks. *Journal of the American Chemical Society* **127**, 5990–5995 (2005).

5. Sammalkorpi, M., Krasheninnikov, A., Kuronen, A., Nordlund, K. & Kaski, K. Mechanical properties of carbon nanotubes with vacancies and related defects. *Physical Review B - Condensed Matter and Materials Physics* **70**, 1–8 (2004).

6. Savin, A. v., Hu, B. & Kivshar, Y. S. Thermal conductivity of single-walled carbon nanotubes. *Physical Review B - Condensed Matter and Materials Physics* **80**, 2498–2499 (2009).

7. Farrera, C., Torres Andón, F. & Feliu, N. Carbon Nanotubes as Optical Sensors in Biomedicine. *ACS Nano* **11**, 10637–10643 (2017).

8. Cheung, W., Pontoriero, F., Taratula, O., Chen, A. M. & He, H. DNA and carbon nanotubes as medicine. *Advanced Drug Delivery Reviews* **62**, 633–649 (2010).

9. Ivanova, M. v., Lamprecht, C., Jimena Loureiro, M., Torin Huzil, J. & Foldvari, M. Pharmaceutical characterization of solid and dispersed carbon nanotubes as nanoexcipients. *International Journal of Nanomedicine* **7**, 403–415 (2012).

10. Katz, E. & Willner, I. Biomolecule-functionalized carbon nanotubes: Applications in nanobioelectronics. *ChemPhysChem* **5**, 1084–1104 (2004).

11. Reuel, N. F. *et al.* Transduction of glycan-lectin binding using near-infrared fluorescent single-walled carbon nanotubes for glycan profiling. *Journal of the American Chemical Society* **133**, 17923–17933 (2011).

12. Satishkumar, B. C. *et al.* Reversible fluorescence quenching in carbon nanotubes for biomolecular sensing. *Nature Nanotechnology* **2**, 560–564 (2007).

13. Ahmed, M., Jiang, X., Deng, Z. & Narain, R. Cationic glyco-functionalized single-walled carbon nanotubes as efficient gene delivery vehicles. *Bioconjugate Chemistry* **20**, 2017–2022 (2009).

14. Muñoz-Bonilla, A. & Fernández-García, M. Glycopolymeric materials for advanced applications. *Materials* **8**, 2276–2296 (2015).

15. Weisman, R. B. Optical Spectroscopy of Single-wall Carbon Nanotubes. (2008).

16. Weisman, R. B. & Bachilo, S. M. Dependence of optical transition energies on structure for single-walled carbon nanotubes in aqueous suspension: An empirical Kataura plot. *Nano Letters* **3**, 1235–1238 (2003).

17. Haddon, R. C. Carbon nanotubes. *Accounts of Chemical Research* **35**, 997 (2002).

18. Tanaka, T., Liu, H., Fujii, S. & Kataura, H. From metal/semiconductor separation to single-chirality separation of single-wall carbon nanotubes using gel. *Physica Status Solidi - Rapid Research Letters* **5**, 301–306 (2011).

19. Ao, G. & Zheng, M. Preparation and separation of DNA-wrapped carbon nanotubes. *Current protocols in chemical biology* **7**, 43–51 (2015).

20. Tu, X., Manohar, S., Jagota, A. & Zheng, M. DNA sequence motifs for structure-specific recognition and separation of carbon nanotubes. *Nature* **460**, 250–253 (2009).

21. Hirano, A., Tanaka, T., Urabe, Y. & Kataura, H. PH-and solute-dependent adsorption of single-wall carbon nanotubes onto hydrogels: Mechanistic insights into the metal/semiconductor separation. *ACS Nano* **7**, 10285–10295 (2013).

22. Ao, G., Streit, J. K., Fagan, J. A. & Zheng, M. Differentiating Left- and Right-Handed Carbon Nanotubes by DNA. *Journal of the American Chemical Society* **138**, 16677–16685 (2016).

23. Stefansson, S., Lazo-Portugal, R., Ahn, S. & Knight, M. Spiral Countercurrent Chromatography Enrichment, Characterization, and Assays of Carbon Nanotube Chiralities for Use in Biosensors. *ACS Omega* **2**, 1156–1162 (2017).

24. Adhikary, A., Kumar, A., Becker, D. & Sevilla, M. D. The guanine cation radical: Investigation of deprotonation states by ESR and DFT. *Journal of Physical Chemistry B* **110**, 24171–24180 (2006).

25. Matta, C. F., Castillo, N. & Boyd, R. J. Extended weak bonding interactions in DNA: π-stacking (base-base), base-backbone, and backbone-backbone interactions. *Journal of Physical Chemistry B* **110**, 563–578 (2006).

26. Miura, Y., Hoshino, Y. & Seto, H. Glycopolymer nanobiotechnology. *Chemical Reviews* **116**, 1673–1692 (2016).

27. Liyanage, S. H. & Yan, M. Quantification of binding affinity of glyconanomaterials with lectins. *Chemical Communications* **56**, 13491–13505 (2020).

28. Dai, Z. *et al.* Nanoparticle-Based Sensing of Glycan - Lectin Interactions. 10018–10019 (2006).

29. Gupta, D., Kaltner, H., Dong, X., Gabius, H. J. & Brewer, C. F. Comparative cross-linking activities of lactose-specific plant and animal lectins and a natural lactose-binding immunoglobulin G fraction from human serum with asialofetuin. *Glycobiology* **6**, 843–849 (1996).

30. Schlick, K. H., Udelhoven, R. A., Strohmeyer, G. C. & Cloninger, M. J. Binding of mannose-functionalized dendrimers with pea (Pisum sativum) lectin. *Molecular Pharmaceutics* **2**, 295–301 (2005).

31. Sharon, N. & Lis, H. How proteins bind carbohydrates: Lessons from legume lectins. *Journal of Agricultural and Food Chemistry* **50**, 6586–6591 (2002).

32. Ando, Y. Carbon nanotube: The inside story. *Journal of Nanoscience and Nanotechnology* **10**, 3726–3738 (2010).

33. Gangoli, V. S., Godwin, M. A., Reddy, G., Bradley, R. K. & Barron, A. R. The State of HiPco Single-Walled Carbon Nanotubes in 2019. *C — Journal of Carbon Research* **5**, 65 (2019).

34. Nguyen, M. A., Ngo, D. T., Le, V. T. & Cao, D. V. Synthesis of single-walled carbon nanotubes over Co-Mo/Al2O 3 catalyst by the catalytic chemical vapor deposition of methane. *Advances in Natural Sciences: Nanoscience and Nanotechnology* **4**, 1–6 (2013).

35. Takakura, A. *et al.* Strength of carbon nanotubes depends on their chemical structures. *Nature Communications* **10**, 1–7 (2019).

36. Mielke, S. L. *et al.* The role of vacancy defects and holes in the fracture of carbon nanotubes. *Chemical Physics Letters* **390**, 413–420 (2004).

37. Kang, J., Al-Sabah, S. & Théo, R. Effect of single-walled carbon nanotubes on strength properties of cement composites. *Materials* **13**, 1–12 (2020).

38. Haggenmueller, R. *et al.* Comparison of the quality of aqueous dispersions of single wall carbon nanotubes using surfactants and biomolecules. *Langmuir* **24**, 5070–5078 (2008).

39. Graf, A. *et al.* Large scale, selective dispersion of long single-walled carbon nanotubes with high photoluminescence quantum yield by shear force mixing. *Carbon* **105**, 593–599 (2016).

40. Pramanik, C., Gissinger, J. R., Kumar, S. & Heinz, H. Carbon Nanotube Dispersion in Solvents and Polymer Solutions: Mechanisms, Assembly, and Preferences. *ACS Nano* **11**, 12805–12816 (2017).

41. Pramanik, D. & Maiti, P. K. DNA-Assisted Dispersion of Carbon Nanotubes and Comparison with Other Dispersing Agents. *ACS Applied Materials and Interfaces* **9**, 35287–35296 (2017).

42. He, M. & Swager, T. M. Covalent Functionalization of Carbon Nanomaterials with Iodonium Salts. *Chemistry of Materials* **28**, 8542–8549 (2016).

43. Stasyuk, O. A., Stasyuk, A. J., Voityuk, A. A. & Solà, M. Covalent Functionalization of Single-Walled Carbon Nanotubes by the Bingel Reaction for Building Charge-Transfer Complexes. *Journal of Organic Chemistry* **85**, 11721–11731 (2020).

44. Safaee, M. M., Gravely, M., Rocchio, C., Simmeth, M. & Roxbury, D. DNA Sequence Mediates Apparent Length Distribution in Single-Walled Carbon Nanotubes. *ACS Applied Materials and Interfaces* **11**, 2225–2233 (2019).

45. Ao, G., Streit, J. K., Fagan, J. A. & Zheng, M. Differentiating Left- and Right-Handed Carbon Nanotubes by DNA. *Journal of the American Chemical Society* **138**, 16677–16685 (2016).

46. Jena, P. v., Safaee, M. M., Heller, D. A. & Roxbury, D. DNA-Carbon Nanotube Complexation Affinity and Photoluminescence Modulation Are Independent. *ACS Applied Materials and Interfaces* **9**, 21397–21405 (2017).

47. Cantwell, M. A., Chan, K. K., Sun, X.-L. & Ao, G. Carbohydrate- and Chain Length-Controlled Complexation of Carbon Nanotubes by Glycopolymers. *Langmuir* (2020) doi:10.1021/acs.langmuir.0c01498.

48. Gao, C. *et al.* Linear and hyperbranched glycopolymer-functionalized carbon nanotubes: Synthesis, kinetics, and characterization. *Macromolecules* **40**, 1803–1815 (2007).

49. Ribeiro, J. P. M., Mendonça, P. v., Coelho, J. F. J., Matyjaszewski, K. & Serra, A. C. Glycopolymer brushes by reversible deactivation radical polymerization: Preparation, applications, and future challenges. *Polymers* **12**, (2020).

50. Xiao, N. Y., Li, A. L., Liang, H. & Lu, J. A well-defined novel aldehyde-functionalized glycopolymer: Synthesis, micelle formation, and its protein immobilization. *Macromolecules* **41**, 2374–2380 (2008).

51. Tang, J. *et al.* Straightforward Synthesis of N-Glycan Polymers from Free Glycans via Cyanoxyl Free Radical-Mediated Polymerization. *ACS Macro Letters* **6**, 107–111 (2017).

52. Godula, K. & Bertozzi, C. R. Synthesis of glycopolymers for microarray applications via ligation of reducing sugars to a poly(acryloyl hydrazide) scaffold. *Journal of the American Chemical Society* **132**, 9963–9965 (2010).

53. Chaganti, L. K., Venkatakrishnan, N. & Bose, K. An efficient method for FITC labelling of proteins using tandem affinity purification. *Bioscience Reports* **38**, 1–8 (2018).

54. Breen, C. J., Raverdeau, M. & Voorheis, H. P. Development of a quantitative fluorescence-based ligand-binding assay. *Scientific Reports* **6**, 1–9 (2016).

55. Fluorescence - Flow Cytometry Guide: Bio-Rad. https://www.bio-rad-antibodies.com/flow-cytometry-fluorescence.html.

56. Yang, S. H. *et al.* Galactosylated manganese ferrite nanoparticles for targeted MR imaging of asialoglycoprotein receptor. *Nanotechnology* **24**, (2013).

57. Pramanik, D. & Maiti, P. K. DNA-Assisted Dispersion of Carbon Nanotubes and Comparison with Other Dispersing Agents. *ACS Applied Materials and Interfaces* **9**, 35287–35296 (2017).

58. Zheng, M. & Diner, B. A. Solution redox chemistry of carbon nanotubes. *Journal of the American Chemical Society* **126**, 15490–15494 (2004).

59. Jang, Y. H. *et al.* pKa values of guanine in water: Density functional theory calculations combined with Poisson-Boltzmann continuum-solvation model. *Journal of Physical Chemistry B* **107**, 344–357 (2003).

60. Schöppler, F. *et al.* Molar extinction coefficient of single-wall carbon nanotubes. *Journal of Physical Chemistry C* **115**, 14682–14686 (2011).

61. Lyu, M., Meany, B., Yang, J., Li, Y. & Zheng, M. Toward Complete Resolution of DNA/Carbon Nanotube Hybrids by Aqueous Two-Phase Systems. *Journal of the American Chemical Society* **141**, 20177–20186 (2019).

62. Khripin, C. Y., Tu, X., Howarter, J., Fagan, J. & Zheng, M. Concentration measurement of length-fractionated colloidal single-wall carbon nanotubes. *Analytical Chemistry* **84**, 8733–8739 (2012).

63. Safaee, M. M., Gravely, M., Rocchio, C., Simmeth, M. & Roxbury, D. DNA Sequence Mediates Apparent Length Distribution in Single-Walled Carbon Nanotubes. *ACS Applied Materials and Interfaces* **11**, 2225–2233 (2019).

64. Zheng, Y., Bachilo, S. M. & Weisman, R. B. Quenching of Single-Walled Carbon Nanotube Fluorescence by Dissolved Oxygen Reveals Selective Single-Stranded DNA Affinities. *Journal of Physical Chemistry Letters* **8**, 1952–1955 (2017).

65. Ao, G., Khripin, C. Y. & Zheng, M. DNA-controlled partition of carbon nanotubes in polymer aqueous two-phase systems. *Journal of the American Chemical Society* **136**, 10383–10392 (2014).

66. Ichinose, Y., Eda, J., Yomogida, Y., Liu, Z. & Yanagi, K. Extraction of High-Purity Single-Chirality Single-Walled Carbon Nanotubes through Precise pH Control Using Carbon Dioxide Bubbling. *Journal of Physical Chemistry C* **121**, 13391–13395 (2017).

67. Chen, X. *et al.* Interfacing carbon nanotubes with living cells. *Journal of the American Chemical Society* **128**, 6292–6293 (2006).

68. Lotan, R., Skutelsky, E., Danon, D. & Sharon, N. The purification, composition, and specificity of the anti T lectin from peanut (Arachis hypogaea). *Journal of Biological Chemistry* **250**, 8518–8523 (1975).

69. Gupta, D. *et al.* A comparison of the fine saccharide-binding specificity of Dioclea grandiflora lectin and concanavalin A. *European Journal of Biochemistry* **242**, 320–326 (1996).

70. Mandeville, J. S. & Tajmir-Riahi, H. A. Complexes of dendrimers with bovine serum albumin. *Biomacromolecules* **11**, 465–472 (2010).

71. Meagher, J. L. *et al.* Crystal structure of banana lectin reveals a novel second sugar binding site. *Glycobiology* **261**, 7306–7310 (2005).

72. Brewer, C. F. & Bhattacharyya, L. Specificity of concanavalin A binding to asparagine-linked glycopeptides. A nuclear magnetic relaxation dispersion study. *Journal of Biological Chemistry* **261**, 7306–7310 (1986).

73. Sun, B., Zhang, Y., Chen, W., Wang, K. & Zhu, L. Concentration Dependent Effects of Bovine Serum Albumin on Graphene Oxide Colloidal Stability in Aquatic Environment. *Environmental Science and Technology* **52**, 7212–7219 (2018).

APPENDIX A: SUPPLEMENTARY INFORMATION: OPTICAL

CHARACTERIZATION OF DNA-WRAPPED SWCNTS AT CONTROLLED PH

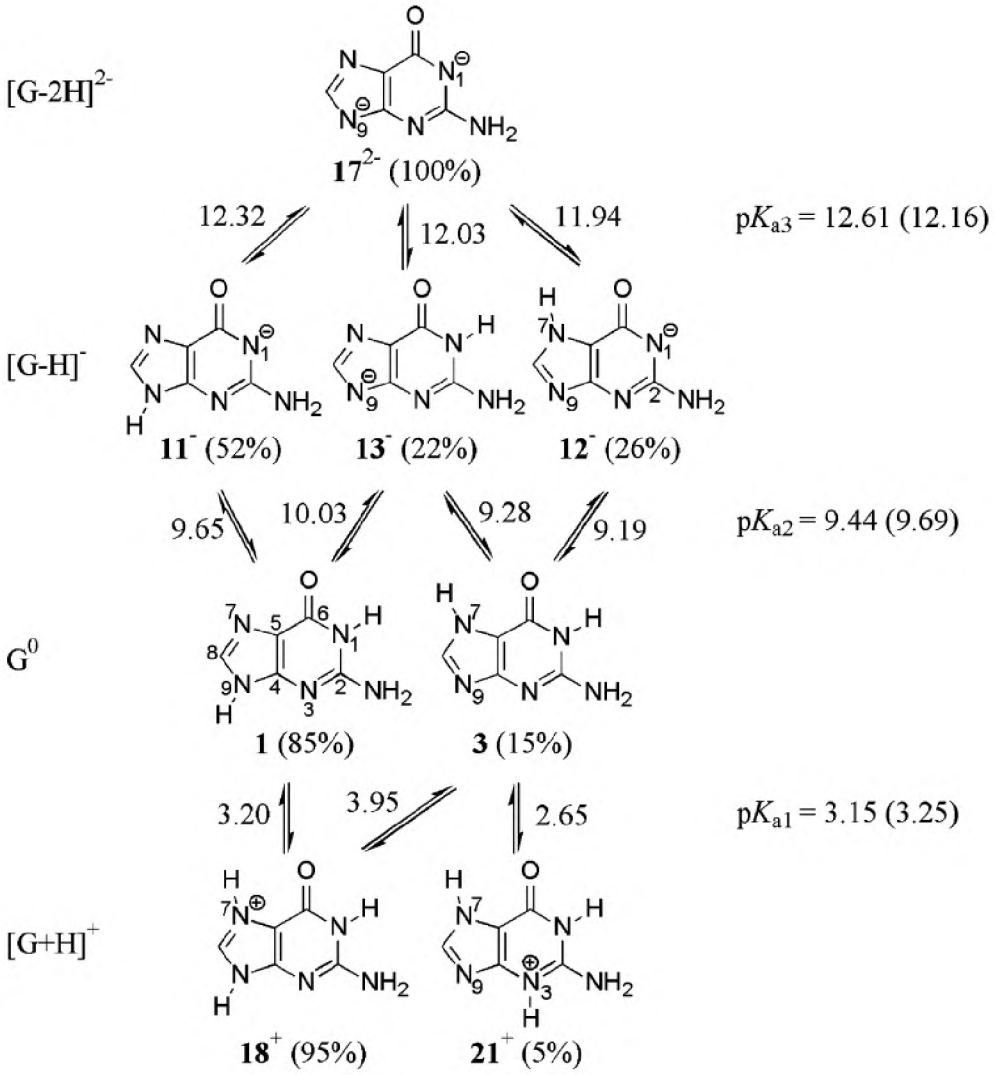

Figure 7.1: Schematic depicting pKa values for major tautomers of guanine in the aqueous phase and their ionization states. Reproduced by Ref (24).

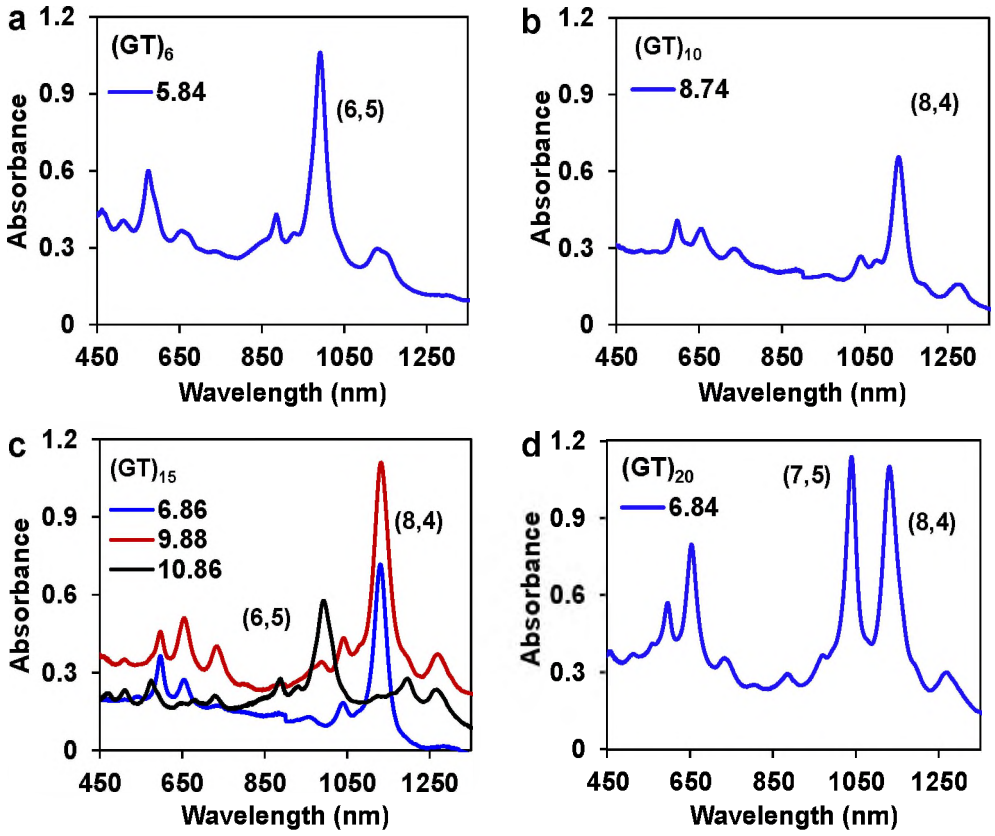

Figure 7.2: (GT)n-SWCNT (n=6,10,15,20) aqueous two-phase extraction of highly enriched single species using PEG/DX with PVP mediator at controlled pH.

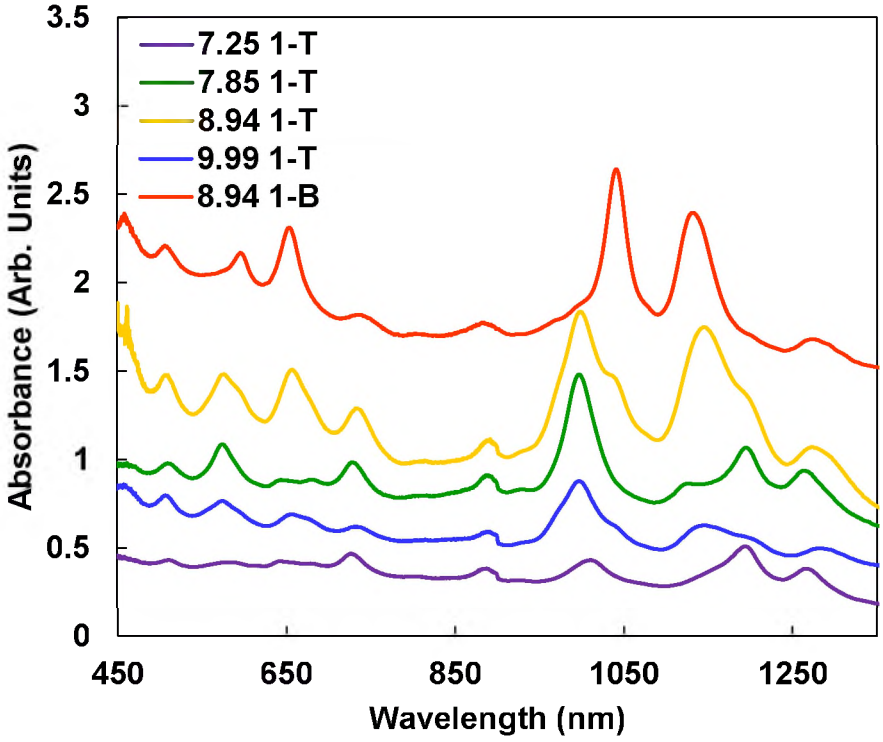

Figure 7.3: CTTC3TTC-wrapped SWCNT aqueous two-phase separation in PEG/DX with PVP mediator at controlled pH shows enriched peaks for (6,5) at pH=7.85, and (7,5) and (8,4) at pH=9.94.

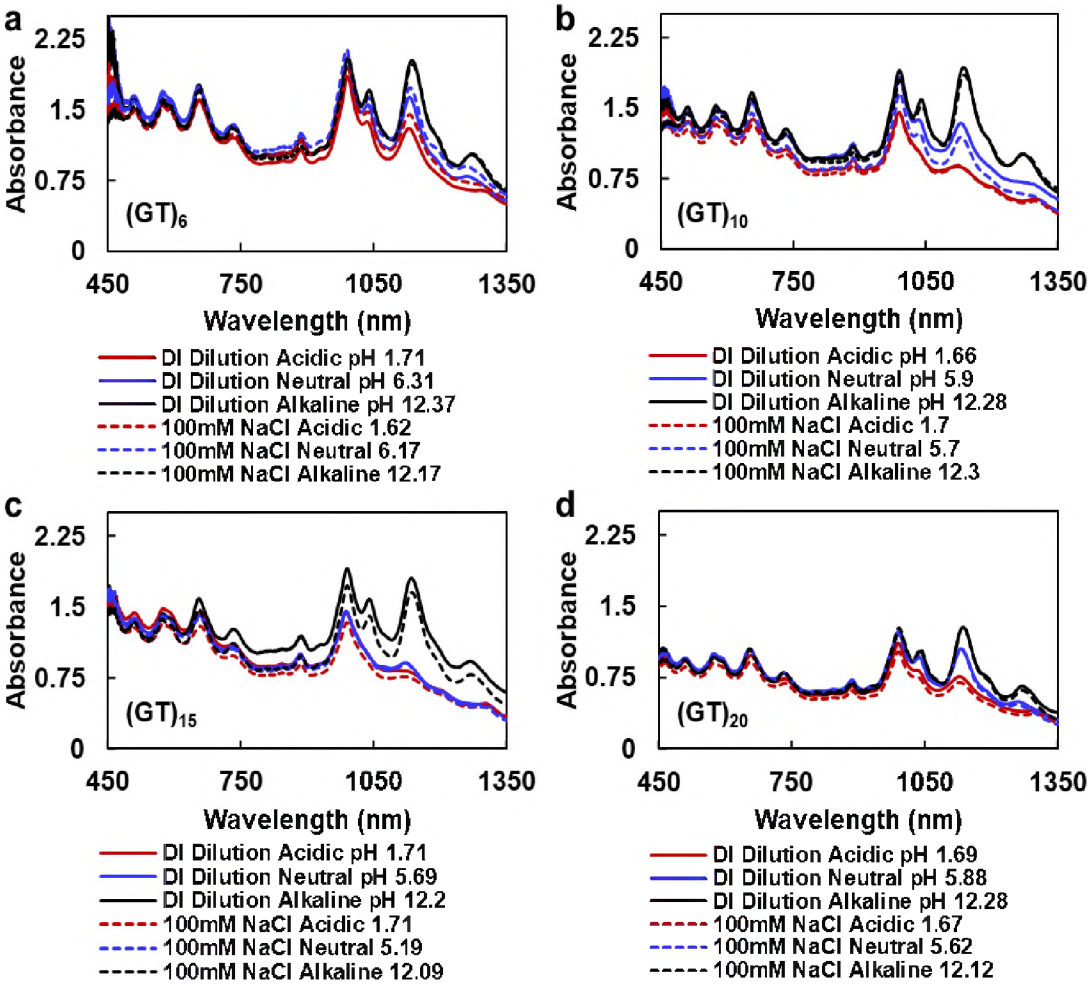

Figure 7.4: $(GT)_n$-SWCNT (n-6, 10, 15, 20) supernatant at acidic, neutral, and alkaline conditions, with and without added NaCl concentration, show that reduction in oxidation potential and tighter DNA wrapping structure is independent of increased ion content at varied pH via absorbance spectra.

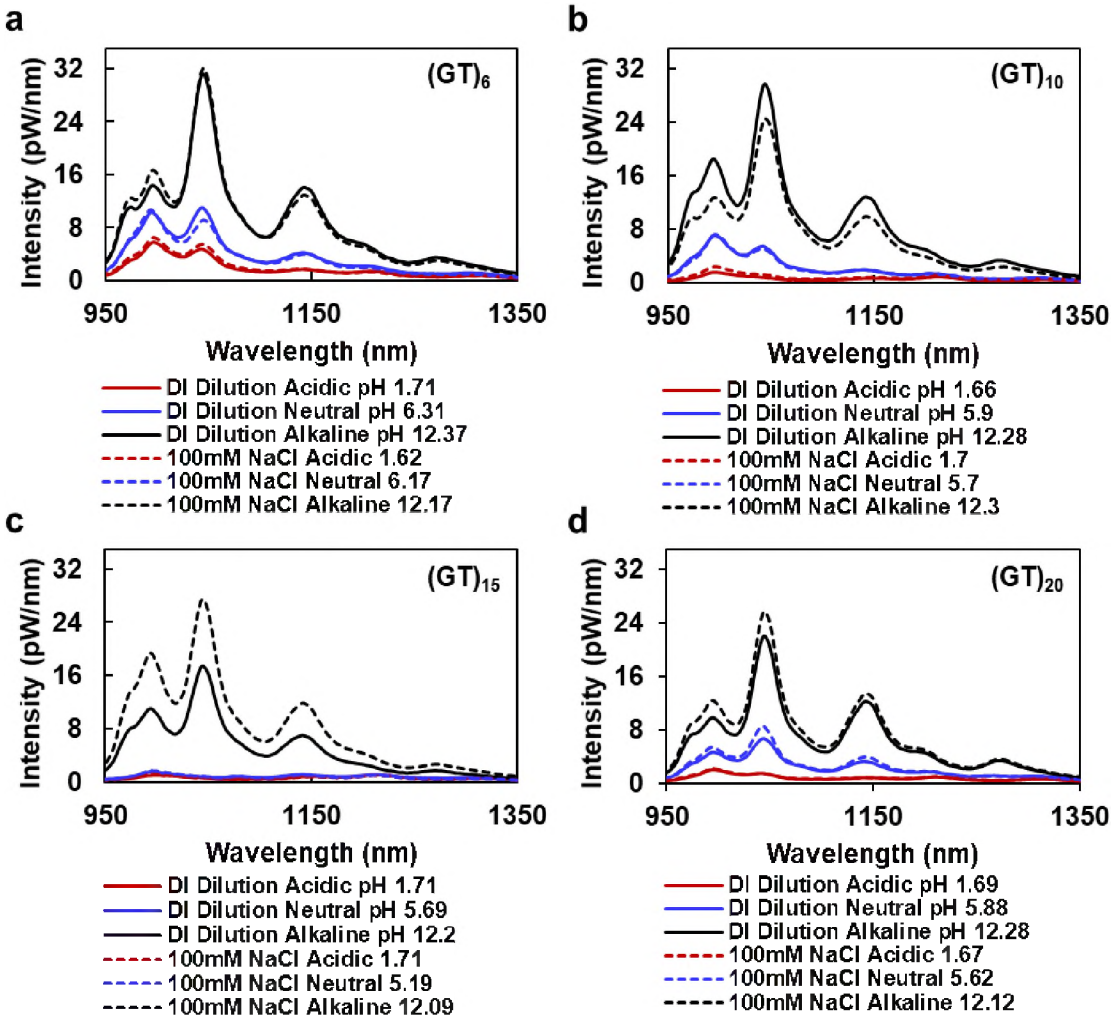

Figure 7.5: $(GT)_n$-SWCNT (n-6, 10, 15, 20) supernatant at acidic, neutral, and alkaline conditions, with and without added NaCl concentration, show that reduction in oxidation potential and tighter DNA wrapping structure is independent of increased ion content at varied pH via NIR fluorescent spectra.

APPENDIX B: SUPPLEMENTARY INFORMATION FOR CARBOHYDRATE-PROTEIN BINDING INTERACTIONS ON NONCOVALENT GLYCO-WRAPPED SINGLE-WALL CARBON NANOTUBE COMPLEXES

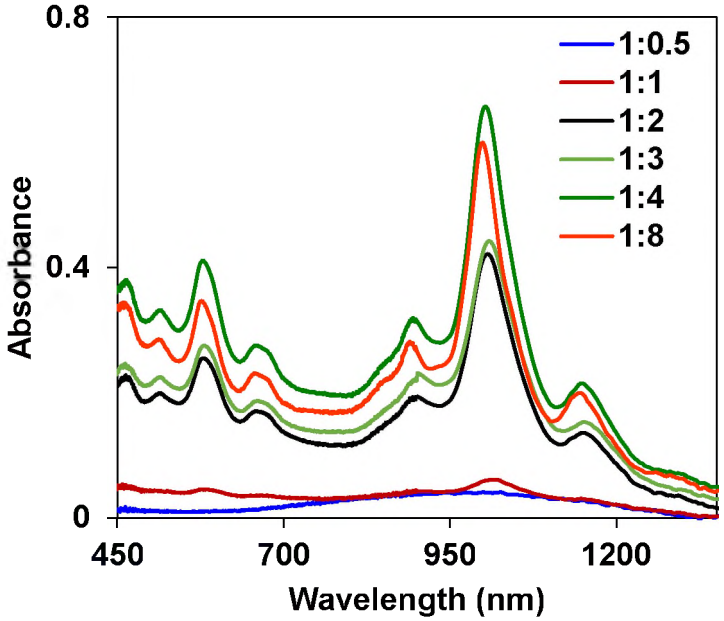

Figure 8.1: Mass ratio analysis of SWCNT:glycopolymer to optimize dispersion conditions.

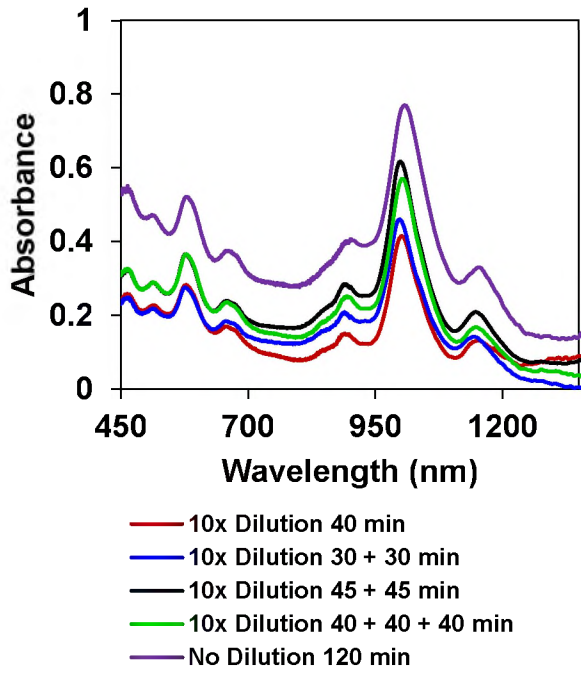

	Conc SWCNTs (mg/mL)
40 min	0.0197
30 + 30 min	0.0296
45 + 45 min	0.0399
40 + 40 + 40 min	0.0342
120 min	0.0067

Figure 8.2: Tip sonication duration analysis to determine optimal dispersion times with corresponding nanotube concentrations.

Table 8.1: Selection of proteins used during this thesis with molecular weight, binding affinity, and solution preparation indicated.

Product Name	MW	Binding Affinity	Storage Temp	Stock Solution
Lectin from Arachis hypogaea-FITC conjugate, lyophilized powder. Sigma-Aldrich, product number L7381	120 kDa	β-gal(1→3)galNAc (galactose)	-20 °C for powder	1 mg/mL in PBS pH 7.3. Specifically, measure 0.1 mg and add 100 µL buffer solution.
Concanavalin A from Canavalia ensiformis (Jack bean), FITC conjugate, Type IV, lyophilized powder. Sigma-Aldrich, product number C7642	102 kDa	α-man (mannose), α-glc (glucose)	-20 °C for powder	1 mg/mL in PBS pH 7.3. Specifically, measure 0.1 mg and add 100 µL buffer solution.
Galanthus nivalis from (snowdrop), lyophilized powder, Sigma-Aldrich, product number L8275	52 kDa	α-man	2-8 °C	1 mg/mL in PBS pH 7.3. Specifically, measure 0.1 mg and add 100 µL buffer solution.
Bovine Serum Albumin, heat shock fraction, protease free, fatty acid free, essentially globulin free, pH 7, ≥98%, lyophilized powder. Sigma-Aldrich, product number A7030	~66 kDa	non-specific binding	2-8 °C	1 mg/mL in PBS pH 7.3. Specifically, measure 0.1 mg and add 100 µL buffer solution.

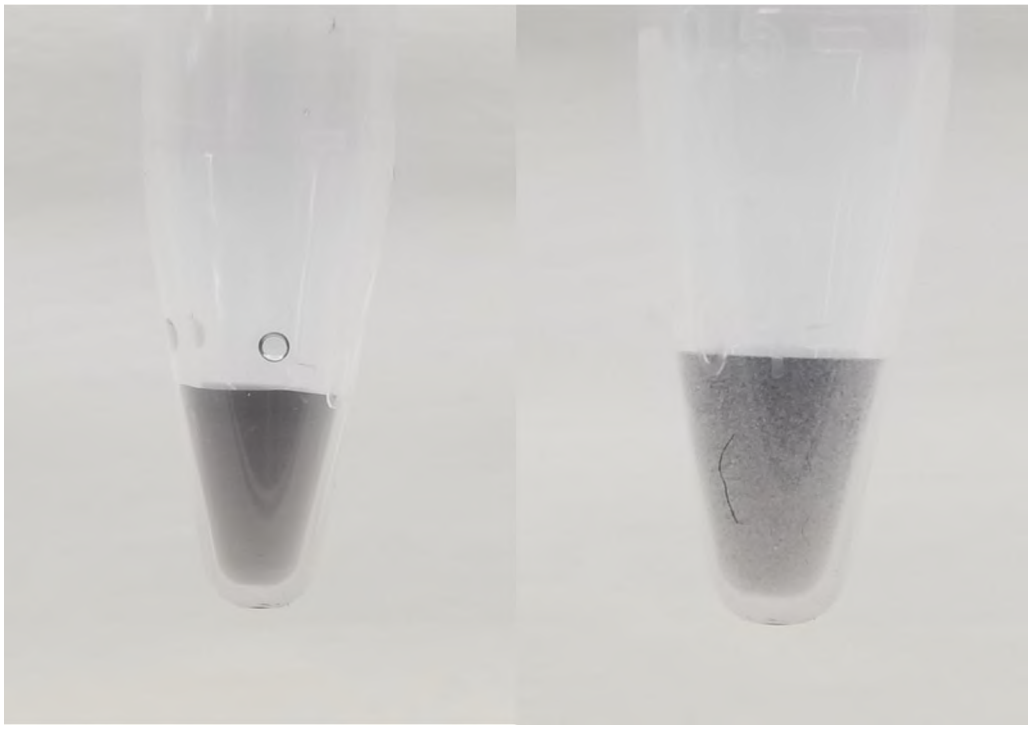

Figure 8.3: Image of Glyco-SWCNT hybrid before PNA addition (left) and after PNA addition (right) depicting the formation of agglomerations due to the cross-linking lattices formed between Glyco-SWCNT hybrids and PNA.

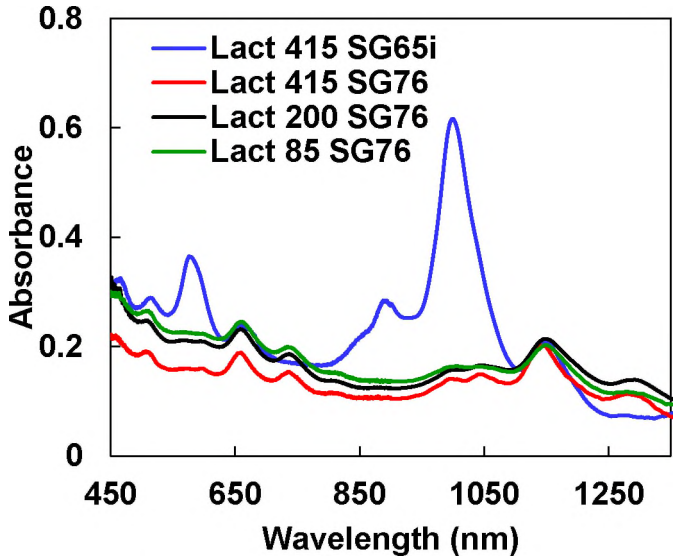

Figure 8.4: Attempts to disperse (7,6) enriched large diameter SWCNTs via disaccharide lactose-containing homopolymers of varying polymer chain length.

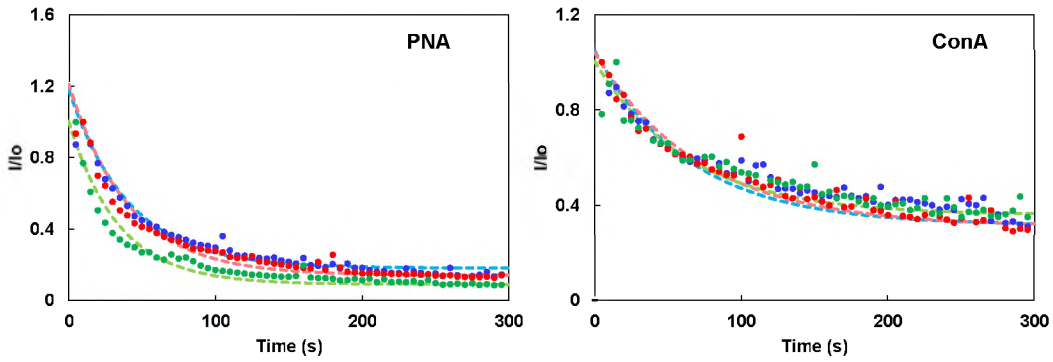

Figure 8.5: Additional kinetic trials for 2.25 ± 0.1 μM PNA and ConA addition to Lact-AM 400-SWCNT hybrids illustrated via dimensionless intensity over 5 minutes and analyzed using single-site adsorption model.

Table 8.2: Analysis of exponential fits of FITC 525 nm intensity ratio $I(t)/I_0$ vs. time using model $\frac{I(t)}{I_0} = A(1 - e^{-k_A t}) + B$ for rate constant (k_A) corresponding to the inverse time constant $1/t$, kinetic coefficient (A), and kinetic correction factor (B) for repetitive trials of ConA and PNA addition to Lact-AM 400-SWCNT complexes.

Lectin	t (s)	A	B	R^2
PNA	38.42±3.26	-0.996±0.066	1.134±0.093	0.966±0.01
ConA	66.34±3.62	-0.702±0.040	1.031±0.019	0.924±0.03